MONITORING ACTIVE VOLCANISM USING ASTER SATELLITE REMOTE SENSING: VOLCÁN DE COLIMA, COLIMA, MEXICO

By

MAGGIE LIN SILVERTOOTH

Bachelors of Science in Geology

Oklahoma State University

Stillwater, Oklahoma

2010

Submitted to the Faculty of the
Graduate College of the
Oklahoma State University
in partial fulfillment of
the requirements for
the Degree of
MASTER OF SCIENCE
December, 2010

MONITORING ACTIVE VOLCANISM USING ASTER SATELLITE REMOTE SENSING: VOLCÁN DE COLIMA, COLIMA, MEXICO

Thesis Approved:

Dr. Jeffrey M. Byrnes

Thesis Adviser

Dr. Anna Cruse

Dr. Eliot Atekwana

Dr. Mark E. Payton

Dean of the Graduate College

ACKNOWLEDGMENTS

The completion of this thesis would not have been possible without the assistance of those who have wholeheartedly believed in my success as a student. I am forever indebted to my adviser Dr. Jeffrey Byrnes. It has been a life-long dream to study volcanoes, and with his guidance I have been able to successfully fulfill this dream. I am forever grateful for the experiences he has given me throughout my time as his graduate student. Without his patience, and willingness to push me not only as a student but also as an individual, I would not feel as successful as I do now.

I would also like to thank Dr. Anna Cruse, Dr. Alex Simms, and Dr. Eliot Atekwana for their unwavering help and support through not only the completion of my Masters degree, but my Bachelors degree as well. I have learned more than I ever imagined possible from their friendship and instruction. I would also like to thank Dr. Jim Puckette for encouraging me to become a Geologist and for every ounce of support that he has provided. Every professor within the Geology Department has played a role in my success and I am forever grateful.

My parents have been two of my biggest supporters. Without their encouragement, patience and un-relenting love with me when I was stressed I would not have made it through the times when I felt like giving up. Thank you. I would also like to thank Jeff Roden and Bay Woods for being there everything. Going through graduate school with your best friends makes the stressful times much more bearable.

Lastly I would like to acknowledge all of the unforgettable friendships and memories that I have made during my time at Oklahoma State University. Being a part of the Geology Department has felt like a home away from home. I will remember what I have learned and the knowledge I have gained and remember those who played a part in such an important part of my life. Thank you.

TABLE OF CONTENTS

LIST OF TABLES

LIST OF FIGURES

INTRODUCTION

Volcán de Colima is an andesitic (52–66% SiO_2) stratovolcano that rises 3,860 m above sea level. Located on the border of the states of Colima and Jalisco (Figure 1), Volcán de Colima is the most active, and considered one of the most dangerous, volcanoes in Mexico (Luhr and Carmichael, 1980). The city of Colima, located 35 km SSW of the volcano, has a population of approximately 130,000 of people; approximately 390,000 people live within a 40 km radius of Volcán de Colima (Gonzalez et al., 2002). With such a large population living in such close proximity to this active volcano, it is important to understand and monitor hazards associated with active volcanism in this area. At Volcán de Colima, the primary hazard is dome collapse; additional hazards include pyroclastic flows, ash fall, lahars, sector collapse, and lava flows. To better understand these hazards, past eruptive cycles can be examined. Volcán de Colima's frequent activity is well-documented (Venzke et al., 2010), and shows constructive and destructive phases that have been described by Varley et al. (2009). Constructive phases are periods of dome growth typically accompanied by frequent, minor explosive activity. There is then a transition period leading to a destructive phase. Destructive phases are characterized by stronger explosive eruptions as well as an event that significantly

decreases the size of the dome or destroys it completely. This destruction can be caused by a large extrusion of lava, an explosion, and/or a collapse of the dome. Monitoring of Volcán de Colima is primarily undertaken by three organizations: Observatorio Vulcanológico (Colima Volcano Observatory) and the Centro de Intercambio e Investigación en Vulcanología (Centre of Exchange and Research in Volcanology) at the University of Colima, and Unidad Estatal de Protección Civil y Bomberos Jalisco (Jalisco State Unit of Civil Protection and Firemen). Monitoring by these organizations predominantly include ground-based efforts, including visual observations, seismic and tilt data, and limited broad-band ground-based thermal data, with limited overflights of the volcano. To supplement these efforts, the goal of this project was to develop an approach for incorporating satellite-based remote sensing analyses using thermal infrared (TIR) data to examine surface temperature and texture, and using visible and near infrared (VNIR) data to examine morphology. The results of this work may also be applied more broadly to monitoring active volcanoes in many parts of the world.

Figure 1: Generalized map showing area of Volcán de Colima, including the state of Colima in relation to Mexico. Volcán de Colima can be seen on the border of the states of Colima and Jalisco. Modified from Luhr (1985).

Objective

The objective of this study is to enhance the understanding of volcanic activity before and after a major eruption in an effort to improve forecasting of volcanic events and assessment of volcanic hazards. To conduct this study, morphologic changes and the constructive and destructive phases of the active lava dome at Volcán de Colima were characterized using data acquired by the Advanced Spaceborne Thermal Emission and Reflection Radiometer (ASTER) instrument (Yamaguchi et al., 1998; Pieri and Abrams, 2004). Available data was collected and analyzed to quantify changes in vesicularity and temperature on the dome and within the crater, and morphologic changes associated with

deposits emplaced on the flanks of the volcano and temporal differences in the size of the lava dome and crater. Changes in vesicularity on the dome and crater can be used to infer conditions before and after eruptions, which include volatile content, flow emplacement, and cooling rate (Ramsey and Fink, 1999). Variations in surface temperature can signify changes in volcanic activity. For example, an increase in temperature may indicate exogenous growth of the lava dome, reflecting extrusion of molten material on the dome surface; whereas a decrease in temperature may indicate endogenous growth, reflecting cooling of the dome surface during growth. Morphologic changes of the dome, crater, and flanks of the volcano allow for the distribution of new deposits to be characterized. This distribution of new material is quantified using ASTER VNIR data and compared with archived reports provided by the Smithsonian Global Volcanism Program (GVP) (Venzke et al., 2010).

ASTER was launched as part of the Terra satellite on December 18, 1999 (Yamaguchi et al., 1998; Pieri and Abrams, 2004). ASTER provides multispectral nadir data at VNIR (3 bands at 15 m/pixel), shortwave infrared (SWIR; 6 bands at 30 m/pixel) and TIR (5 bands at 90 m/pixel) wavelengths and one backward-looking VNIR band to provide stereo coverage (Table 1). ASTER data has been found to be useful for volcanologic investigations (e.g., Byrnes et al., 2004; Pieri and Abrams, 2004; Ramsey and Dehn, 2004) as well as a wide range of other applications (Welch et al., 1998; Yamaguchi et al., 1998). The Terra satellite follows a Sun-synchronous, nearly polar orbit slightly more than 30 minutes behind the Landsat 7 satellite, allowing ASTER to have a repeat time of 16 days, although data for a particular target is generally collected much less frequently (Yamaguchi et al., 1998; Pieri and Abrams, 2004). The primary objective of the ASTER

mission is to improve the understanding of local- and regional-scale processes that occur on, or near, the Earth's surface and lower atmosphere, which also includes surface-atmosphere interactions (Yamaguchi et al., 1998). ASTER was designed to acquire repetitive, multispectral data over the VNIR, SWIR, and TIR portions of the electromagnetic spectrum. Table 1 lists the band number and spatial resolution of the three wavelength regions in which data are acquired. ASTER provides opportunities for observing volcanoes and their activity from low Earth orbit and is unique because ASTER is a targeted instrument. This requires a fundamentally new approach toward the management of data acquisition requests as it provides the first pointable, multispectral, and stereo coverage (Pieri and Abrams, 2004). For the purpose of this study, only the VNIR and TIR bands were examined due to the usefulness of VNIR bands to observe changes in morphology, and TIR bands to detect changes in surface temperature and small-scale texture, such as vesicularity (Yamaguchi et al., 1998; Ramsey and Fink, 1999; Byrnes et al., 2004).

Table 1. Summary of ASTER subsystems (Yamaguchi et al., 1998).

Subsystem	Band Number (wavelength range)	Spatial Resolution
VNIR	1 (0.52 - 0.60 µm)	15 m/pixel
	2 (0.63 - 0.69 µm)	
	3N, nadir-looking (0.76 - 0.86 µm)	
	3B, backward-looking (0.76 - 0.86 µm)	
SWIR	4 (1.600 - 1.700 µm)	30 m/pixel
	5 (2.145 - 2.185 µm)	
	6 (2.185 - 2.225 µm)	
	7 (2.235 - 2.285 µm)	
	8 (2.295 - 2.365 µm)	
	9 (2.360 - 2.430 µm)	
TIR	10 (8.125 - 8.475 µm)	90 m/pixel
	11 (8.475 - 8.825 µm)	
	12 (8.925 - 9.275 µm)	
	13 (10.25 - 10.95 µm)	
	14 (10.95 - 11.65 µm)	

Previous Work

Previous studies have used satellite remote sensing to further understanding of thermal anomalies, changes in emissivity (a material property), and morphological changes associated with volcanoes. Research has shown that data from Landsat Satellites with spatial resolution less than 100 m/pixel can provide information on surface conditions and magmatic events (Francis and Rothery, 2000). Pieri and Abrams (2004) demonstrated that images provided by the Landsat Thematic Mapper could be used to

determine the temperature of eruptions and the locations of fumaroles. It is now possible to observe changes more frequently and at higher spatial resolution, as well as being able to have detailed observations of domes, lava flows and geothermal activity.

Additional studies on monitoring volcanic activity with thermal data include using the Advanced Very High Resolution Radiometer (AVHRR) to look at thermal wavelengths greater than 3 µm (Oppenheimer and Rothery, 1991). This work examined rock surface and fumarole vents and illustrated the potential to detect and measure surface temperatures of these bodies. Using remote sensing, the ability to measure surface roughness can be obtained. Ramsey and Fink (1999) explored this by measuring the emissivity of silicate rocks and determining the surface vesicularity of volcanic rocks on Medicine Lake, a large shield volcano located northeast of Mount Shasta in northern California. The goal of their study was to use the Thermal Infrared Multispectral Scanner (TIMS) to estimate the surface vesicularity of rhyolite flows in the area. The vesicularity of silicate rocks is characterized by a decrease in emissivity at a wavelength range of 8-10 µm (Ramsey and Fink, 1999). Volcanic glass (i.e., obsidian) is shown to contain two features in the 7-25 µm wavelength region, where the first occurs between 8 and 12 µm and the other occurs between 20 and 25 µm. Such spectral signatures can be used to quantify small-scale roughness, such as vesicularity, of volcanic rocks (Ramsey and Fink, 1999).

A similar study was carried out by Byrnes et al. (2004) for a basaltic lava flow field. Surface units in the Mauna Ulu flow field, Kilauea Volcano, Hawaii, were examined through field and remote sensing analyses. ASTER and MASTER (MODIS/ASTER airborne simulator) were used in order to detect spectral characteristics of the Mauna Ulu

surface units to determine whether the surface units could be differentiated (Byrnes et al., 2004). It was determined that differences in morphologies and surface textures produced by differences in lava flow emplacement could be characterized using VNIR and TIR data from each instrument.

BACKGROUND

Tectonic History of Mexico

Mexico is divided into seven morphotectonic provinces, as follows: (1) Sierra Madre del Sur, (2) Sierra Madre Oriental, (3) Gulf Coastal Plain Belt, (4) Sierra Madre Occidental, (5) Sonoran Basin and Range, (6) California Peninsula, and (7) Trans-Mexican Volcanic Belt (TMVB) (Figure 2). Of these, Volcán de Colima is located at the intersection of the Sierra Madre del Sur, TMVB, and the Sierra Madre Occidental (Guzman and Cserna, 1963). The TMVB is a continental volcanic arc that measures almost 1000 km long and stretches across central Mexico from the Gulf of California to the Gulf of Mexico (Luhr and Carmichael, 1980). The TMVB formed due to the subduction of the Cocos Plate at the Middle America Trench; the Cocos Plate is intersected by the Rivera Plate (Figure 2) (Luhr and Carmichael, 1980). The TMVB forms the northern boundary of the Sierra Madre del Sur province and the southern boundary of the Sierra Madre Occidental. This area is made up of Pliocene to Recent cinder cones, lava flows, and pyroclastic flows that are predominantly basaltic in composition (Guzman and Cserna, 1963). The Sierra Madre Occidental is a volcanic plateau consisting of Tertiary lavas, ignimbrites, and tuffs that are predominantly andesitic in composition (Guzman and Cserna, 1963).

Figure 2: General morphotectonic map of Mexico, showing Volcán de Colima within the TMVB. Volcanism in this area is due to the Cocos plate being subducted at the Middle America Trench. This area is intersected by the Rivera Plate, forming a triple junction. Modified from Luhr and Charmichael (1980) and Guzman and Cserna, (1963).

Colima Volcanic Complex

The Colima Volcanic Complex (CVC) is located in the western part of the TMVB. This region is located to the east of the intersection of the Rivera Plate and Cocos Plate (Figure 2). Volcán de Colima is located in the Colima Graben, which is bound to the north and the east by a continental triple junction (Luhr et al., 1985; Garduno and Tibaldi, 1990; Macias, 2007). This graben extends 90 km south from the triple junction and is directly above the subduction of the Cocos and Rivera Plates, which accounts for volcanism in this area (Luhr et al., 1985). A chain of three volcanoes makes up the CVC: Volcán Cantaro, Nevado de Colima, and Volcán de Colima (Robin et al., 1987). The three volcanic centers are Quaternary in age but display different magmatic processes (Luhr and Carmichael, 1980; Luhr et al., 1985; Robin, et al., 1987). The oldest caldera, Volcán Cantaro, formed ~0.53 to 0.1 Ma with the growth of a dacitic dome (Robin et al., 1987). Cantaro's growth ended with caldera collapse. Activity at Nevado de Colima started approximately 200,000 years ago and exhibited explosive eruptions as Nevado transitioned from dacitic to andesitic melt (Robin et al., 1997). The most recent, Volcán de Colima exhibits andesitic volcanism. Deposits found around the volcano suggest an age ranging from 9,300 to 400 years (Robin et al., 1997).

Eruptive History

Volcán de Colima's well-documented historical eruptions date back to the 1500's; earlier reports are based on separate accounts and vary in reliability (Gonzalez et al., 2002). Historical documentation of a possible eruption by Volcán de Colima was first

documented in *Nahuatl* culture mythology (Gonzalez et al., 2002). A significant portion of the documentation and writings of this time were destroyed during the Spanish conquest. The earliest accurate account of the volcano's activity can be found in Historia Antigua de Mexico, written by Clavijero in 1780. In this, writings describe the destructive results of the activity of the volcano from 1519 to 1523 (Gonzalez et al., 2002). The first scientific documentation of Colima's activity was reported in 1576. Since this report, Colima has experienced multiple cycles of long-term eruptive activity, typically lasting ~100-150 years and ending with a Plinian eruption (Luhr and Carmichael, 1980). Plinian-type explosions contain large quantities of gas, dust, ash, and incandescent lava fragments that are blown out of a central crater and produce a high convection column (Walker, 1973). Within these long-term cycles of activity, seven major eruptions since 1576 have occurred: 1585, 1606, 1685, 1818, 1913, 1994, and 2005 (Gonzalez et al., 2002). The 1818 eruption was the largest of the 19th century. In 1869 significant lava flows were first documented as part of an eruption at Volcán de Colima. The volcano experienced an increase in activity from 1899 to 1902 with more than 1000 eruptions reported (Gonzalez et al., 2002). An eruption in 1913 signaled the end of this eruptive period; the volcano was again relatively quiet until the current cycle of activity started in 1961 with effusive eruptions (Luhr and Carmichael, 1980; Abrams et al., 1991; Gonzalez et al., 2002). Large explosions have occurred during the current cycle in 1994 and 2005, as well as large effusive events in 1991, 1998, and 2004 (Gonzalez et al., 2002). The eruptions occurring in 2005 are the strongest recorded in the current eruptive cycle (Varley et al., 2009).

Lava Dome Phases

According to Luhr and Carmichael (1980), long-term eruptive cycles begin with a slow, discontinuous piston-like ascent of a lava dome into an open crater. Within these long-term cycles, shorter-term phases of dome growth and destruction occur, typically lasting 50 to 140 years. Constructive phases of dome growth alternate with destructive phases until the culmination of the eruptive cycle in a Plinian eruption, such as in 1611, 1818, and 1913 (Luhr and Carmichael, 1980). Destructive phases may diminish or destroy the lava dome, and may include effusion of blocky lava flows (seen in 1576, 1749, 1869 1961, and 1975) and pyroclastic flows (including Peléan-style eruptions), rockfalls, and Vulcanian eruptions (Luhr and Carmichael, 1980; Robin et al., 1991; Varley et al., 2009; N. Varley, personal communication, 2010).

Constructive and destructive phases reflect variations in magmatic processes, including volatile content, rate and extent of magma degassing, pressure changes, and rate at which magma moves through the conduit (Robin et al., 1991; Varley et al., 2009, N. Varley, personal communication, 2010). Constructive effusive phases are characterized by slow ascending magma that is low in volatiles. A lava dome is formed and continues to grow until the dome reaches the crater rim, spilling over and resulting in blocky lava flows (leading to the destructive phase) (Robin et al., 1991). Destructive phases are characterized by strong explosive eruptions or large lava effusions, typically resulting in the destruction of the dome and upper areas of the crater and cone. This general cycle is illustrated in Figure 3. Each of the effusive eruptions contains homogeneous andesitic flows (Robin et al., 1987). Additionally, minor activity at Volcán de Colima includes fumaroles, fracturing of rocks, minor ash cloud eruptions, and rock falls (Abrams et al.,

1991). When explosive activity peaked in 2005, thirty Vulcanian style eruptions were recorded, with each one producing pyroclastic material (Varley et al., 2009). Explosive eruptions in Colima are thought to be triggered when magma quickly ascends, undergoing rapid degassing and crystallization near the surface, causing the existing lava dome to be destroyed (Varley et al., 2009; N. Varley, personal communication, 2010). Additional information on eruptive patterns of Volcán de Colima is provided by Cruz-Reyna (1993).

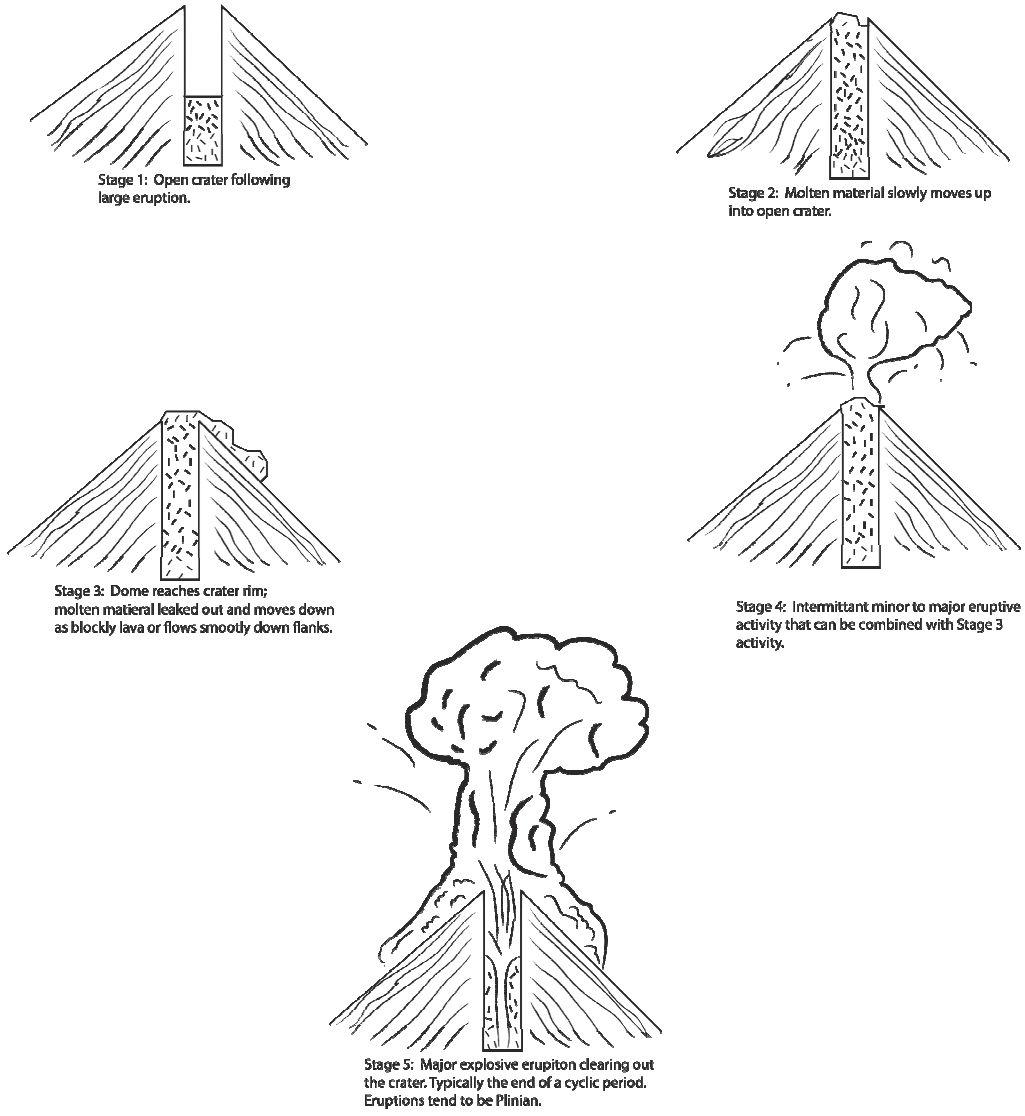

Figure 3: Phases of lava dome growth and destruction; modified from Luhr (2002). Long-term eruptive cycle begins with an open crater (Stage 1). Alternating constructive and destructive phases (Stages 2-4) continue throughout the eruptive cycle, which eventually ends with a Plinian eruption (Stage 5).

METHODOLOGY

Throughout a volcano's activity, steam, gas, and heat are emitted and can be detected with satellite-based sensors, including ASTER. ASTER data is distributed by the Land Processes Distributed Active Archive Center (LP DAAC), located at the U.S. Geological Survey (USGS) Earth Resources Observation and Science (EROS) Center (lpdaac.usgs.gov) and was accessed via NASA's Warehouse Inventory Search Tool (WIST) (EOSDIS, 2010). Scenes of interest were selected based on the amount of cloud cover and coverage of the volcano and surrounding area. The goal was to collect as many possible scenes within the period from 2003 to 2009 in order to observe any changes leading up to, and following, the 2005 activity. Data processing and geospatial analysis were conducted using the ENVI (http://www.ittvis.com/) and ArcMap (http://www.esri.com/) software packages. All collected scenes were georeferenced in ArcMap; using ENVI, regions of interest (ROIs) representing the extents of the crater and dome were determined using VNIR data.

Vesicularity

ASTER TIR and VNIR data were used for calculating vesicularity, specifically emissivity (a standard ASTER level-2 product derived from the 5 TIR bands) and VNIR reflectance (a standard ASTER level-2 product derived from the 3 VNIR bands) data. To calculate vesicularity, TIR data was subsampled from 90 m/pixel to 15 m/pixel using the nearest neighbor technique to spatially correspond directly to the VNIR pixels. Each VNIR image was then overlaid on the corresponding resampled TIR image. ROIs representing the extents of the crater and dome were determined for each scene, illustrating the subtle changes in the crater and dome between acquired scenes.

Statistics were run on the ROIs for band 12 (8.925 - 9.275 μm) in each scene, to show minimum, maximum, and mean emissivity. Statistics pertaining to the crater included the dome (when present) because it is within the crater, however statistics of the dome exclude outlying areas of the crater. Vesicularity was derived from the TIR-derived emissivity data and based on a linear scaling model developed by Ramsey and Fink (1999). Two endmember scalings were used to provide reasonable constraints on surface vesicularity. Vesicularity (V) was scaled based on ASTER band 12 data between an emissivity (ε) value equaling one (representing 100% vesicularity) and some minimum emissivity value (representing 0% vesicularity). For the first endmember, the value for the minimum emissivity is the minimum value in the ASTER band 12 data found in all ROIs ($\varepsilon = 0.788$). The linear scaling is therefore:

$$V = (\varepsilon - 0.788)/(1 - 0.788)$$

The second endmember scaling uses a minimum emissivity value derived from laboratory measurements of obsidian ($\varepsilon = 0.690$) (Ramsey and Fink, 1999). The linear scaling is:

$$V = (\varepsilon - 0.690)/(1 - 0.690)$$

These two data scalings should reasonably constrain the surface vesicularity because the first scaling (based on the ASTER data) should underestimate true vesicularity because it is unlikely that any TIR pixel covered an area with 0% vesicularity, whereas the second scaling (based on laboratory data) should overestimate true vesicularity because the band depths measured in a laboratory setting are not achievable with a spaceborne sensor. Variations in vesicularity of silicate flows are caused by volatile distribution as well as lava emplacement and cooling history (e.g., Ramsey and Fink, 1999; Byrnes et al., 2004). Vesicularity can be used to constrain pre-eruption conditions because it is a function of the volatile content, emplacement time, and the internal structure of the flow.

Temperature

To determine the minimum, maximum, and mean temperature for the crater and dome (when dome is present), the previously described ROIs were used to calculate statistics based on the ASTER kinetic temperature data, which is a standard ASTER level-2 product derived from the five TIR bands.

Morphological Changes

Examination of VNIR reflectance data shows the extent and distribution of volcanic deposits, such as pyroclastic flows, lava flows, rock falls, and lahars that typically occur prior to, as well as sometimes after, major eruptions. To determine changes around the volcano, including emplacement of new deposits, erosion of older deposits, and changes in the shape of the crater and dome, flows from the earliest scene were mapped. Subsequent flows were then identified to map temporal changes in the edifice surface. It should be noted that all flow materials, including pyroclastic deposits, rock fall deposits, lahar deposits, and lava flows, have been grouped because they can not consistently be accurately distinguished based on available ASTER data. The maximum diameter of the crater and lava dome (if applicable) were measured for each scene. To supplement this study, the Smithsonian GVP's archived reports (Venzke, et al., 2010) were used to supply more information about new activity or reports of a growing lava dome. Although the Smithsonian reports may not always detail all activity at the volcano (N. Varley, personal communication, 2010), they do represent a consistent, published source of information that is based on observations.

RESULTS

Lava Dome Vesicularity

Figure 4 shows the calculated dome vesicularity based on the two scalings previously described. The highest maximum values occurred on April 9, 2005, February 26, 2007, March 16, 2008, and December 13, 2008. Overall the highest maximum vesicularity calculated on the dome occurred on March 16, 2008 and December 13, 2008 with values of 93%. The lowest minimum values occurred on March 19, 2003, November 22, 2006, March 30, 2007, and November 14, 2009. The lowest value was calculated to be 37% on March 19, 2003.

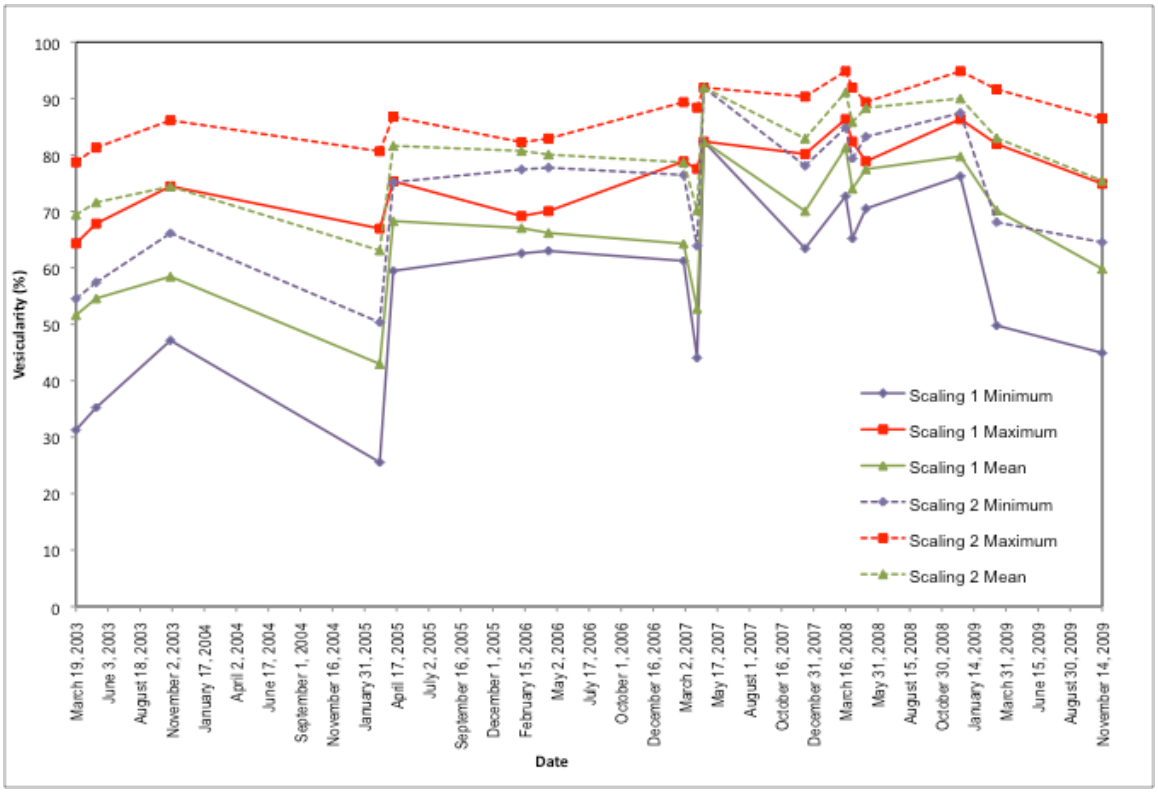

Figure 4: Plot of lava dome vesicularity, March 19, 2003 to November 14, 2009.

Crater Vesicularity

Figure 5 shows vesicularity calculated within the crater, including the dome. The highest maximum values occurred on April 9, 2005, February 26, 2007, March 16, 2008, and December 13, 2008. Overall the highest maximum vesicularity calculated in the crater occurred on March 16, 2008 and December 13, 2008 with values of 94%. The lowest values occurred on March 19, 2003, November 22, 2006, March 30, 2007, and November 14, 2009. The lowest calculated percentage was 54% on March 19, 2003.

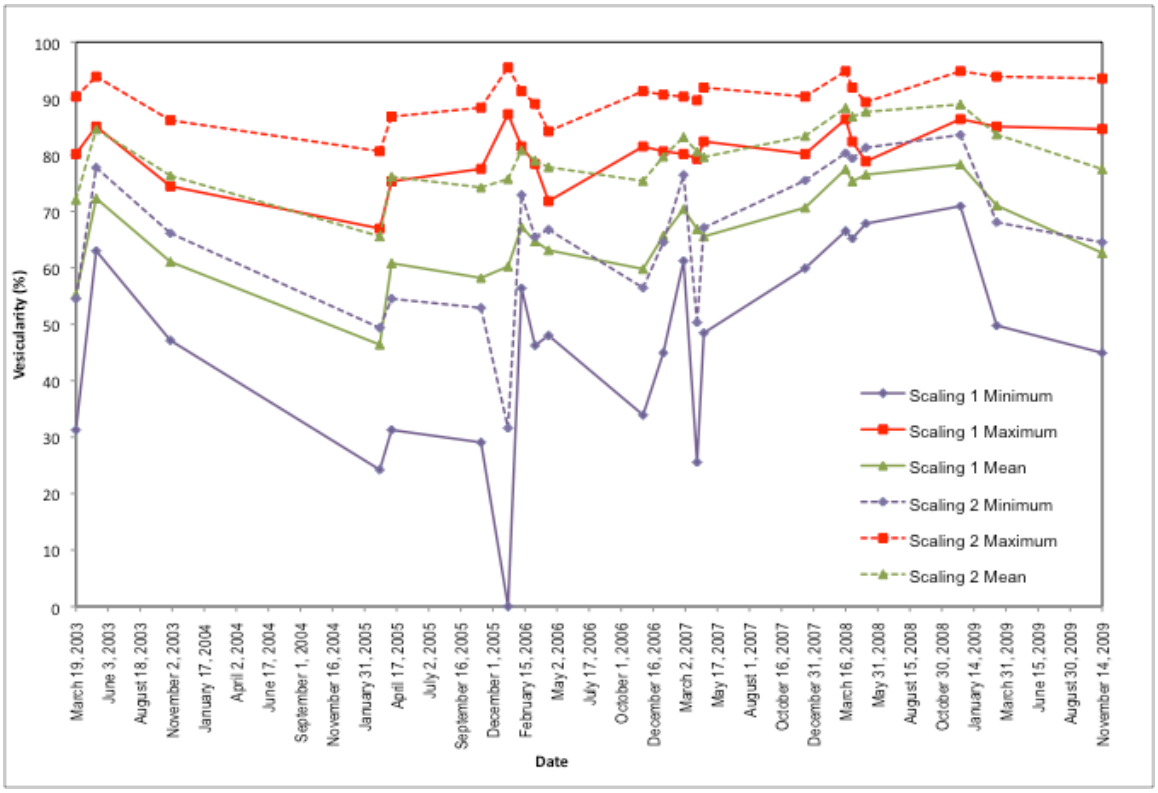

Figure 5: Plot of crater vesicularity (including the lava dome, when present), March 19, 2003 to November 14, 2009.

Lava Dome Temperature

Figure 6 illustrates an overall decreasing trend in minimum and maximum temperature after April 9, 2005. The highest maximum temperatures occurred on April 9, 2005, April 12, 2006, March 30, 2007, and April 1, 2008. The lowest minimum temperatures occurred on February 7, 2006, February 27, 2007, December 11, 2007, and November 14, 2009. The highest maximum temperature on the dome was 366 K on April 9, 2005 and the lowest minimum temperature was 280 K on December 11, 2007.

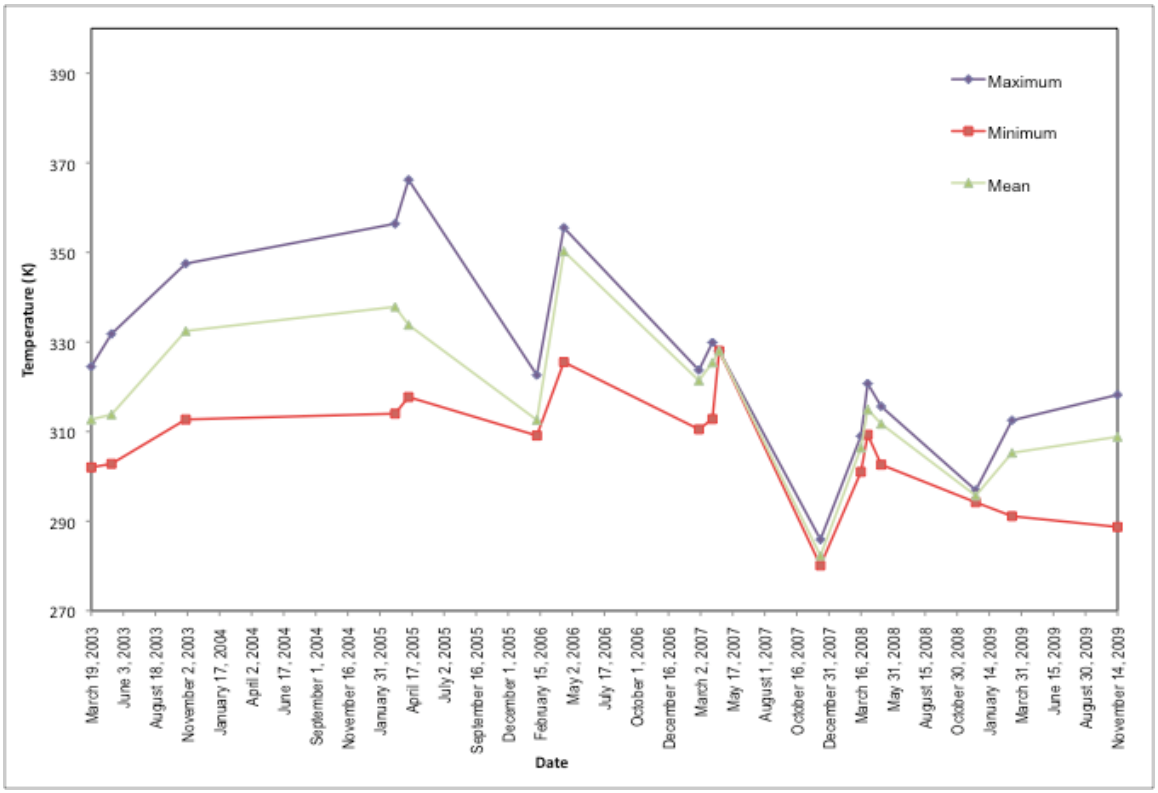

Figure 6: Plot of lava dome temperature, March 19, 2003 to November 14, 2009.

Crater Temperature

Figure 7 shows very distinct temperature highs and lows occurring throughout the study period. Maximum temperatures occurred on May 6, 2003, November 3, 2005, November 22, 2006, April 15, 2007, and May 3, 2008. Minimum temperatures occurred on March 8, 2005, March 11, 2006, February 26, 2007, and March 16, 2008. The highest temperature recorded within the crater was 382 K on May 6, 2003 and the lowest temperature recorded was 277 K on March 16, 2008.

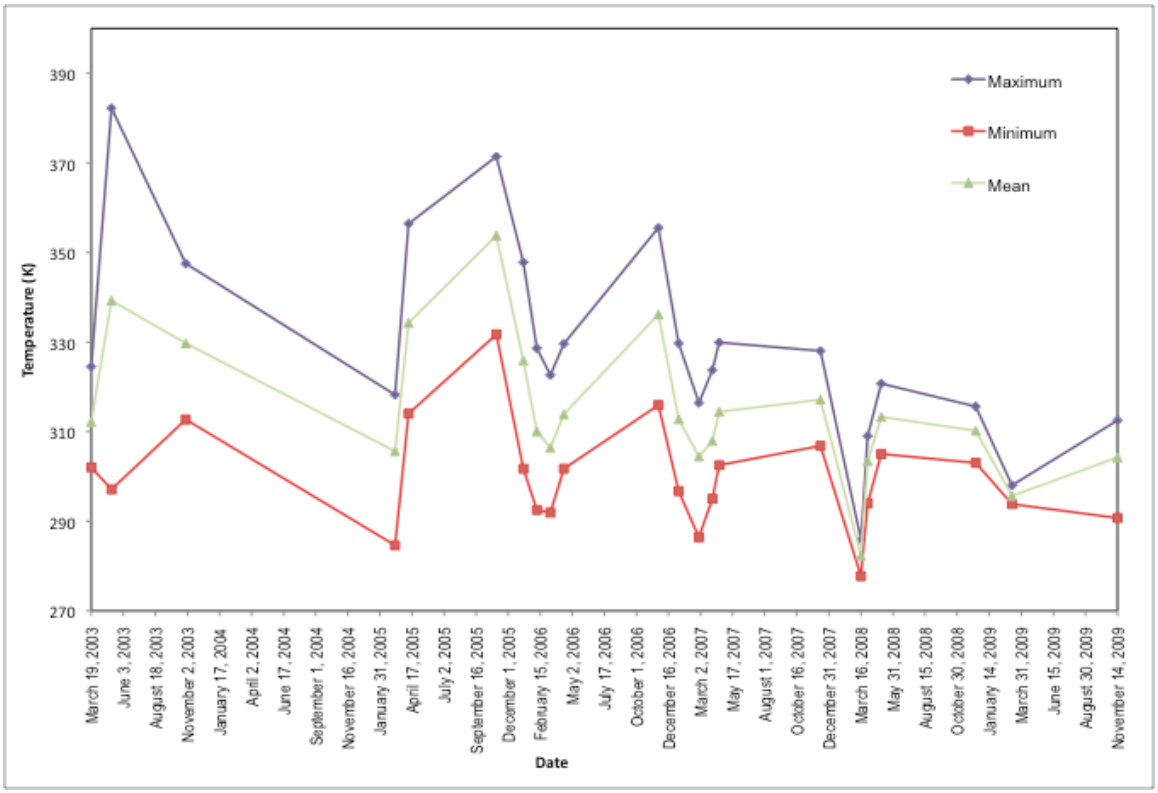

Figure 7: Plot of crater temperature (including the dome), March 19, 2003 to November 14, 2009.

Morphological Changes

Morphological changes are illustrated using ASTER VNIR reflectance data (Figures 8-19, Appendix I). Color figures are shown as composites of band 3 (red), band 2 (green), and band 1 (blue); maps are displayed on ASTER VNIR bases of the most recent scene used for the sequence, shown as a greyscale version of the original color image. Observations based on the mapping are included in the figure captions for the corresponding maps.

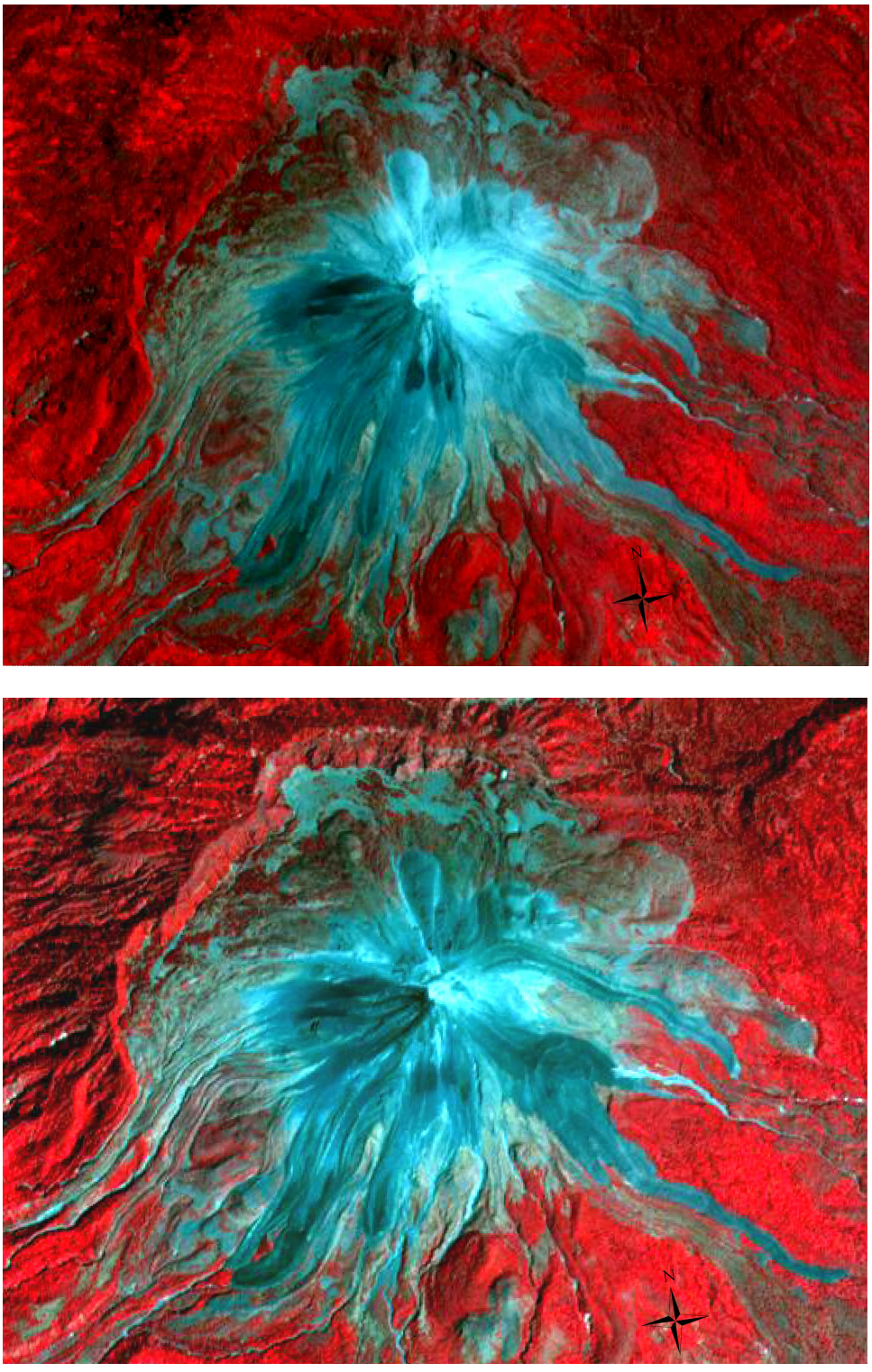

Figure 8: ASTER VNIR images: March 19, 2003 (top), May 6, 2003 (bottom).

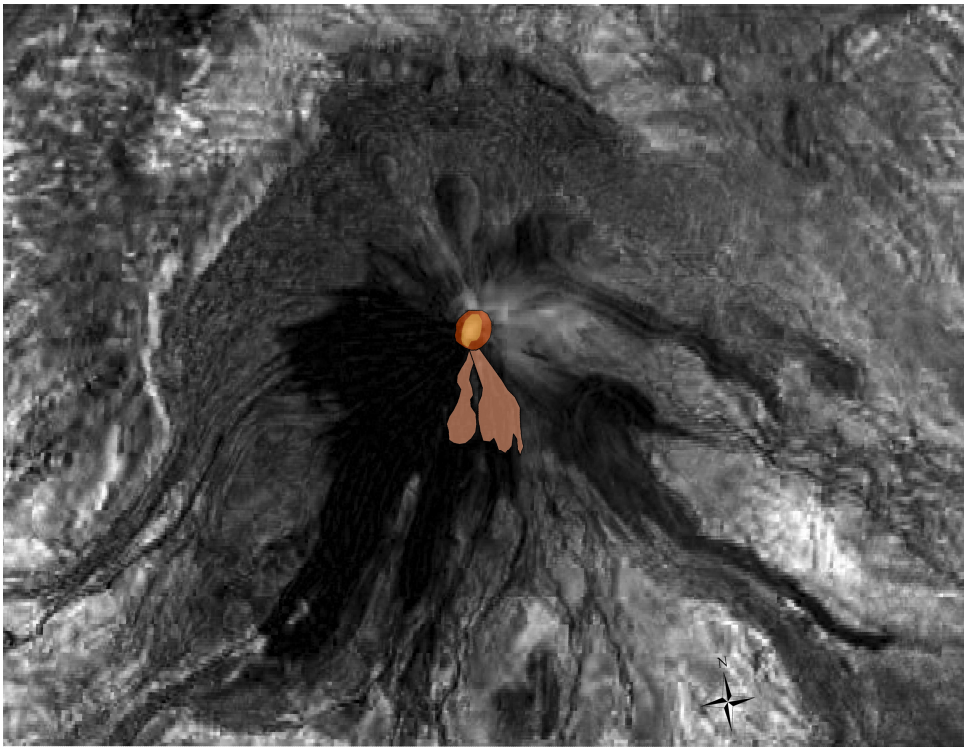

Figure 9: Map of changes that occurred between the previous pair of images (Figure 8). The lava dome measured 108 m in March 19, 2003 and expanded to 275 m in May 6, 2003. The dome is outlined in yellow and the crater is outlined in orange. Two new flows were reported during the span of the previous six weeks (Venzke et al., 2010), which are outlined in red.

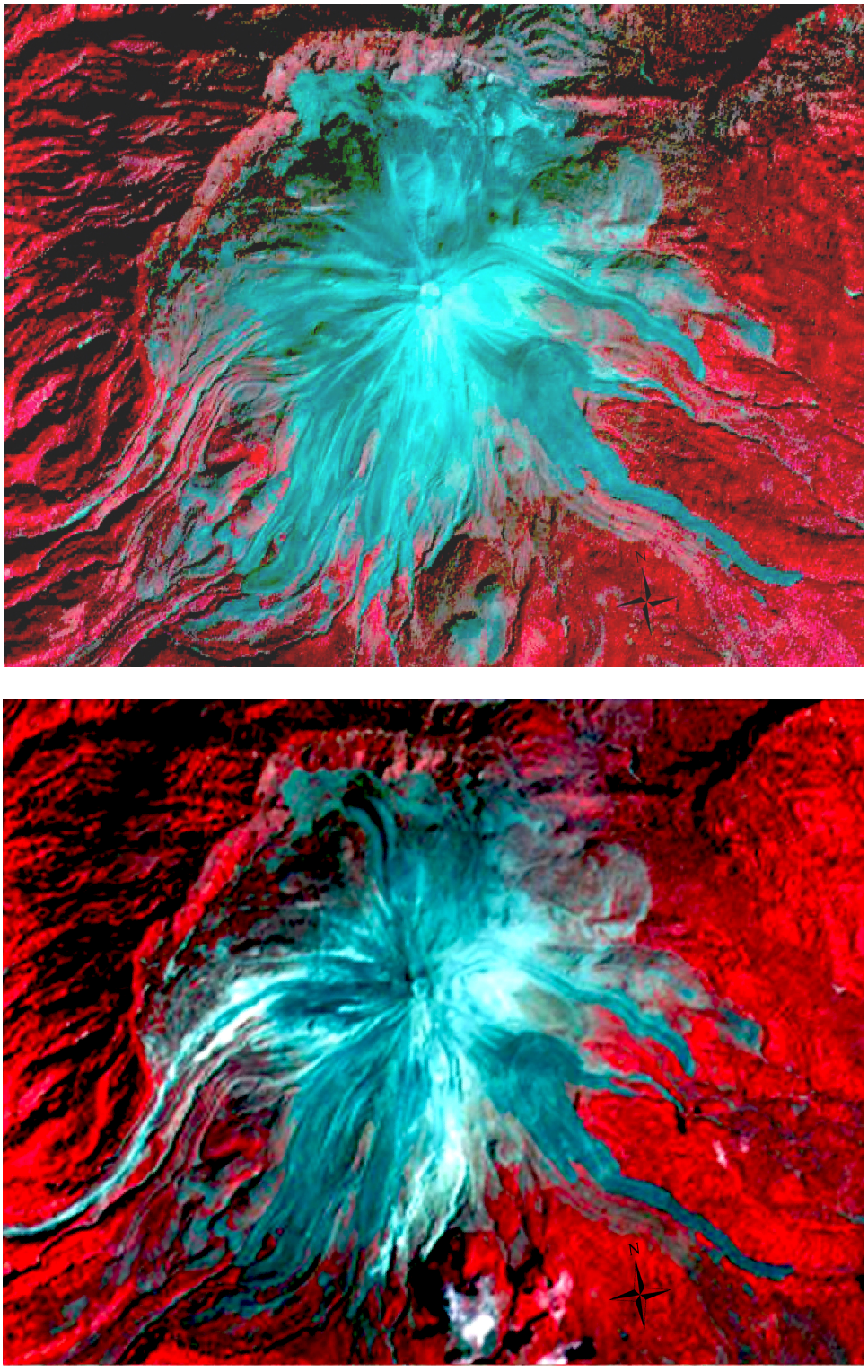

Figure 10: ASTER VNIR images: October 29, 2003 (top), March 8, 2005 (bottom).

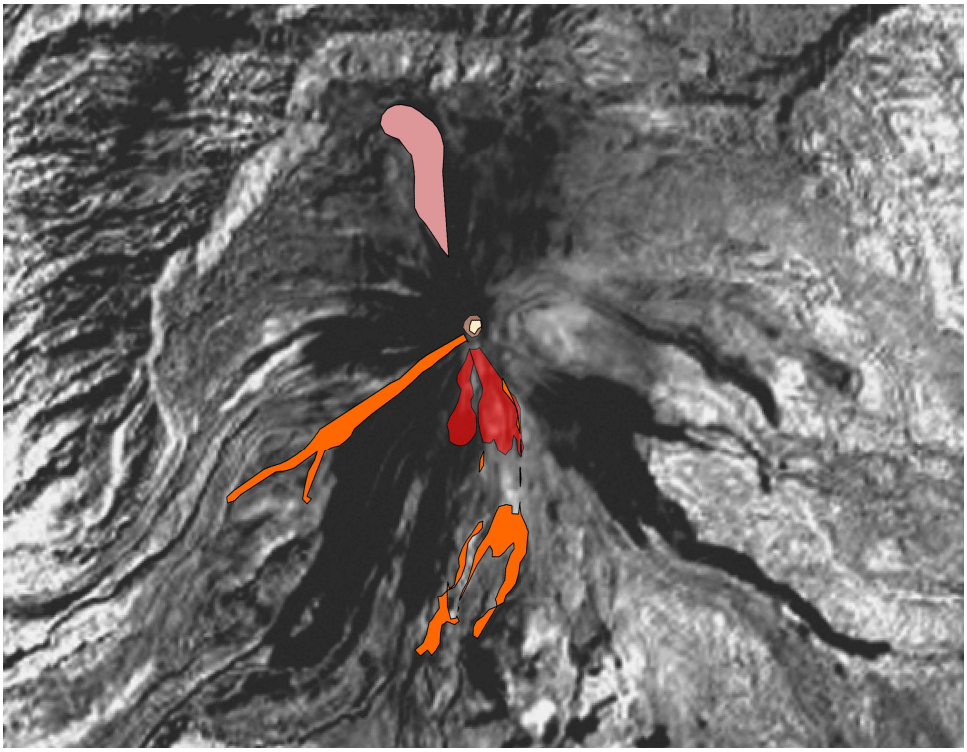

Figure 11: Map of changes that occurred between the previous pair of images (Figure 10). The growing lava dome is outlined in pale yellow and crater is outlined in orange. A new flow occurred in 2004 and is outlined in pink (Venzke et al., 2010); subsequent deposits are outlined in bright orange.

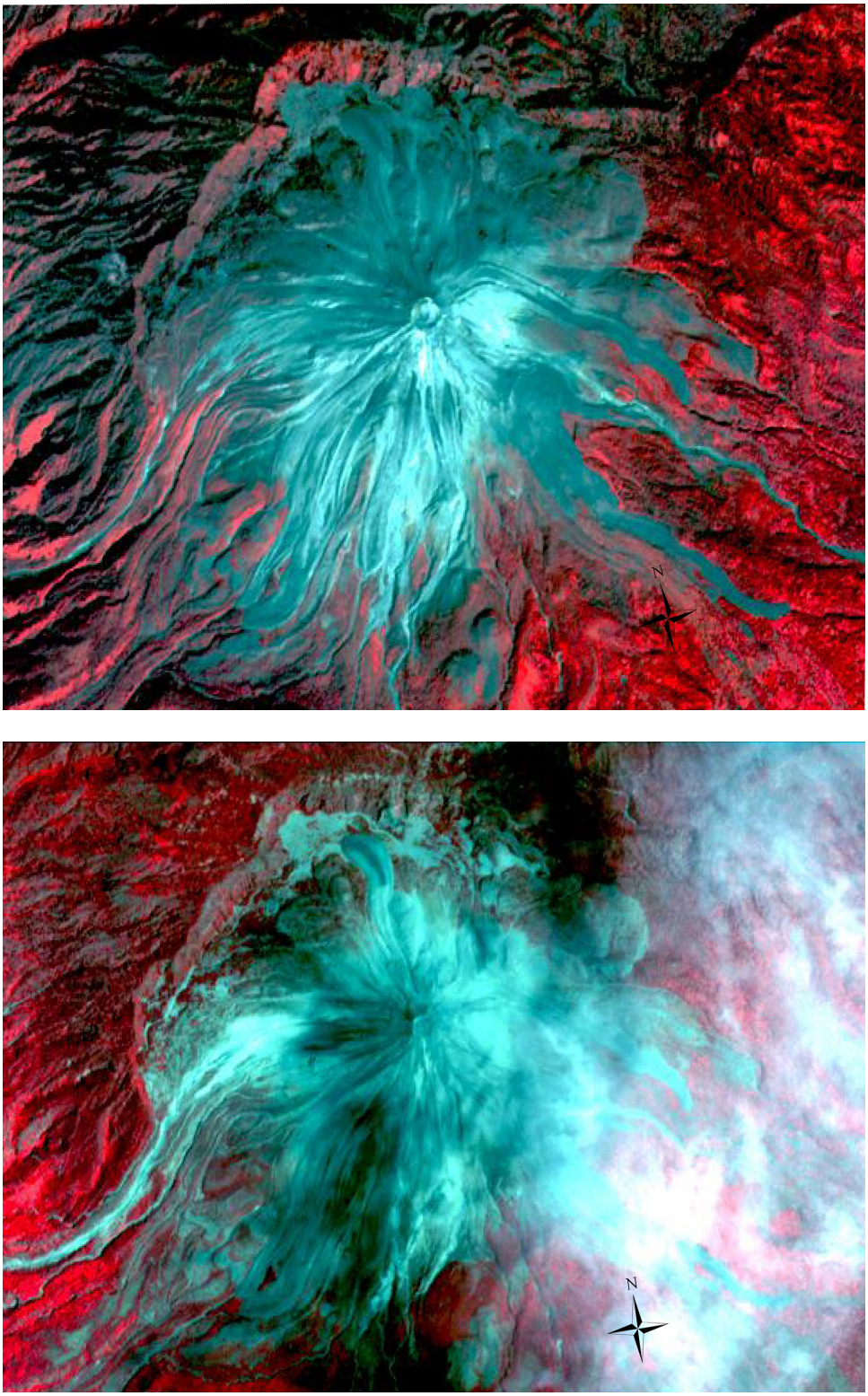

Figure 12: ASTER VNIR images: April 9, 2005 (top), November 3, 2005 (bottom).

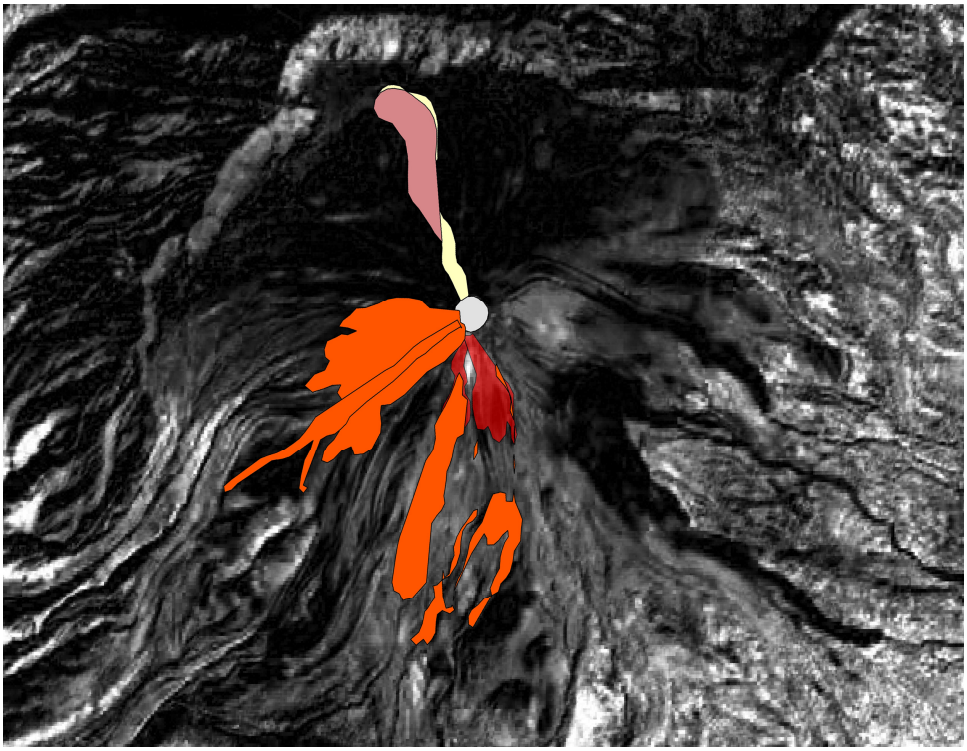

Figure 13: Map of changes that occurred between the previous pair of images (Figure 12). The lava dome that measured 128 m in diameter on April 9, 2005 was destroyed in the June 2005 eruption. The crater is outlined in pale purple. There is no dome; the 2004 flow is outlined in pink as well as newer flows in pale yellow. Subsequent flows are outlined in orange.

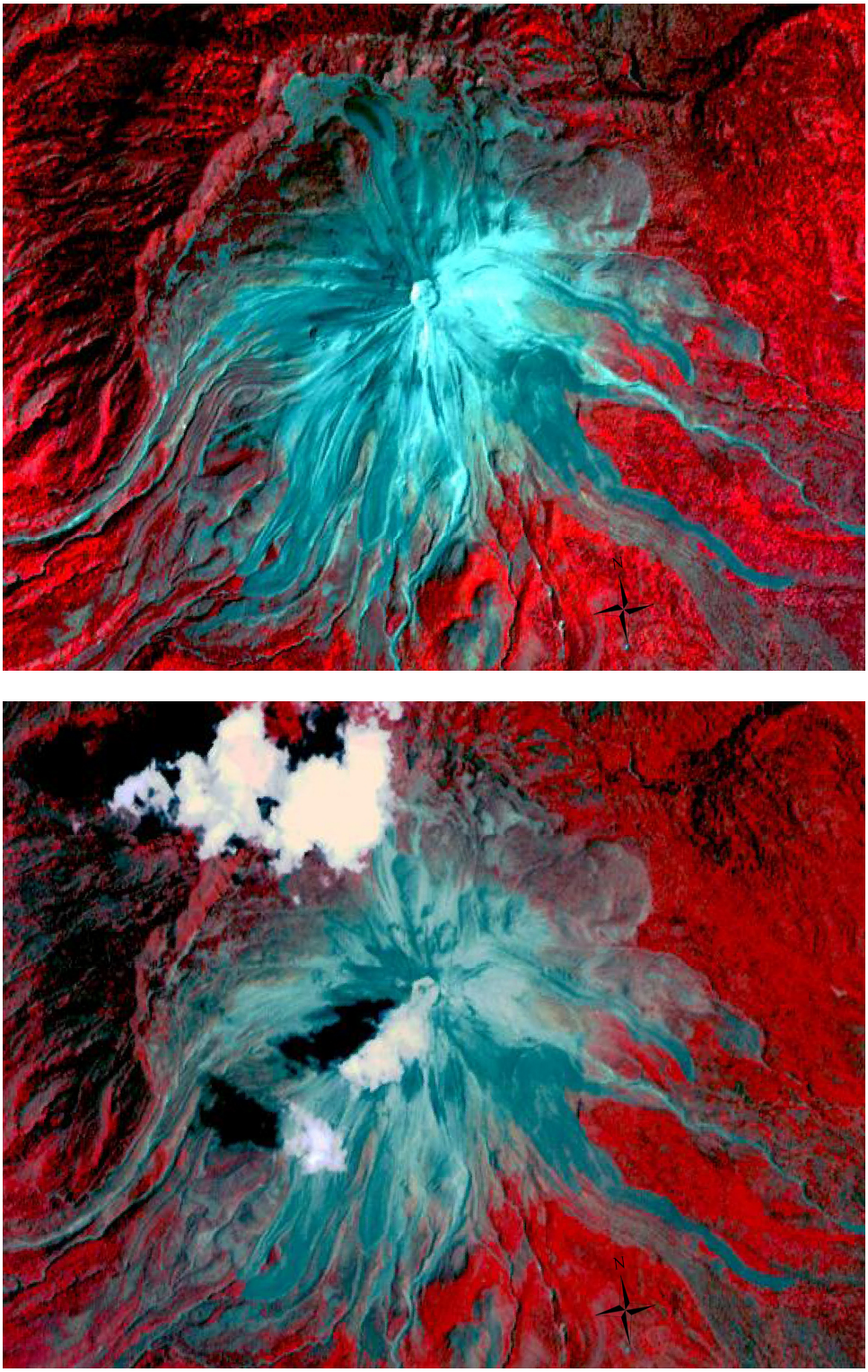

Figure 14: ASTER VNIR images: March 11, 2006 (top), April 12, 2006 (bottom).

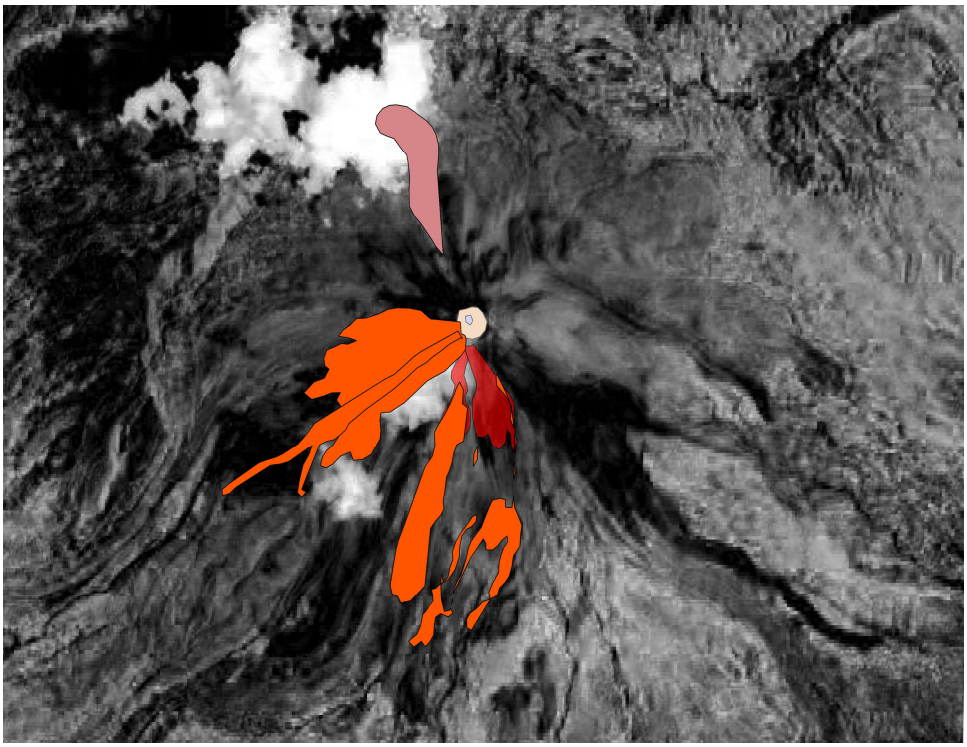

Figure 15: Map of changes that occurred between the previous pair of images (Figure 14). The lava dome was not visible in March 11, 2006; however, it started a period of re-growth and measured 78 m in April 12 2006. The new dome is outlined in pale purple. The crater is outlined in tan; the 2004 flow is outlined in pink. Subsequent flows are outlined in orange.

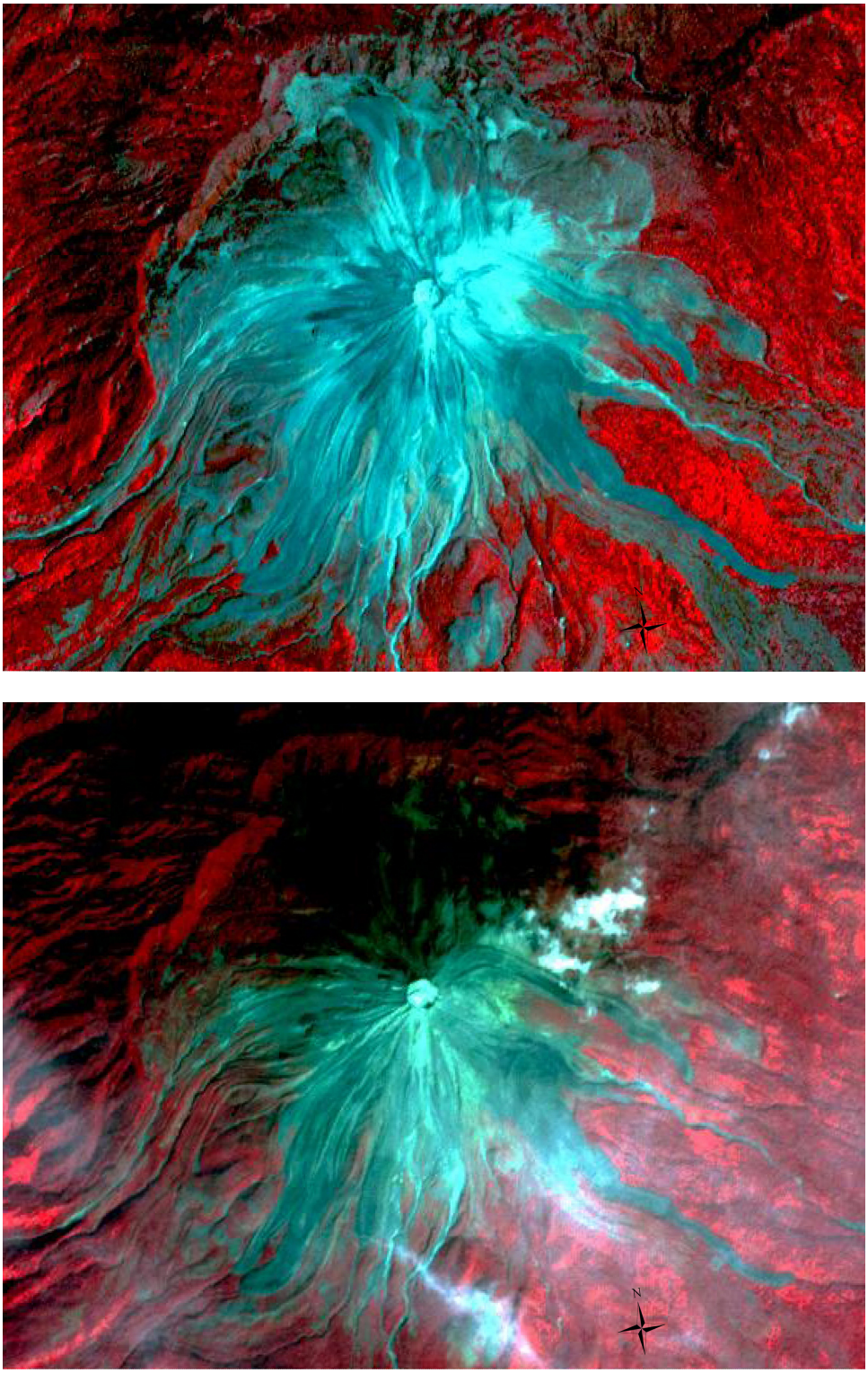

Figure 16: ASTER VNIR images: March 30, 2007 (top), December 11, 2007 (bottom).

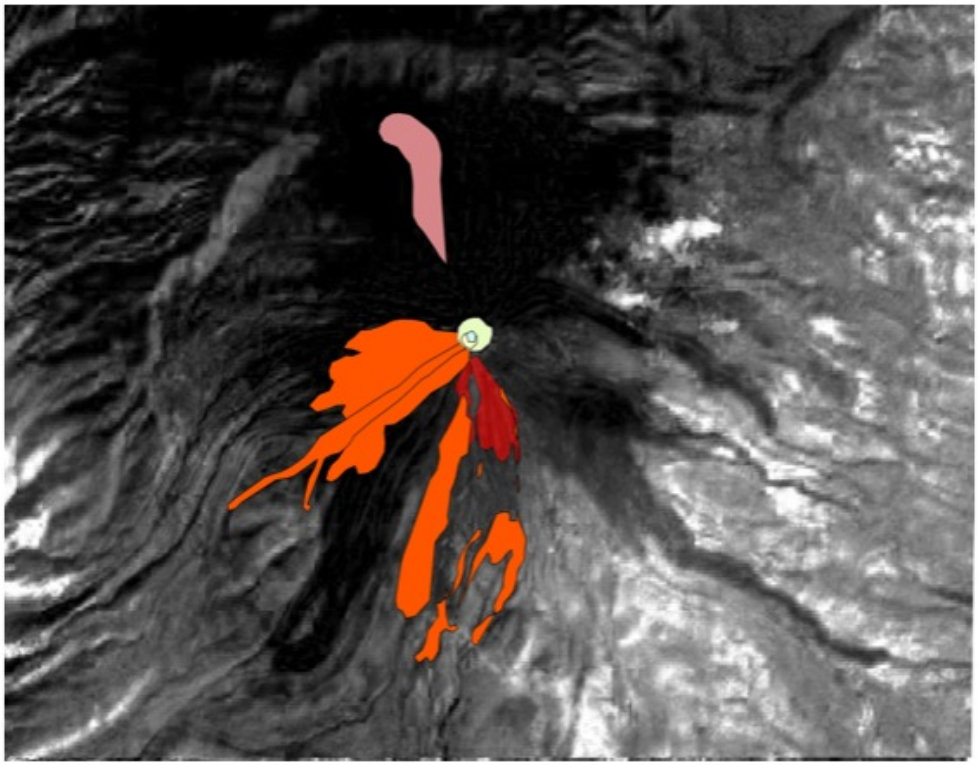

Figure 17: Map of changes that occurred between the previous pair of images (Figure 16). The lava dome was not detectable until March 30, 2007; it measured 95 m and is outlined in light blue. In December 11, 2007, the dome grew to 142 m and is outlined in pale yellow. The crater is outlined in tan; the 2004 flow is outlined in pink. Subsequent flows are outlined in orange.

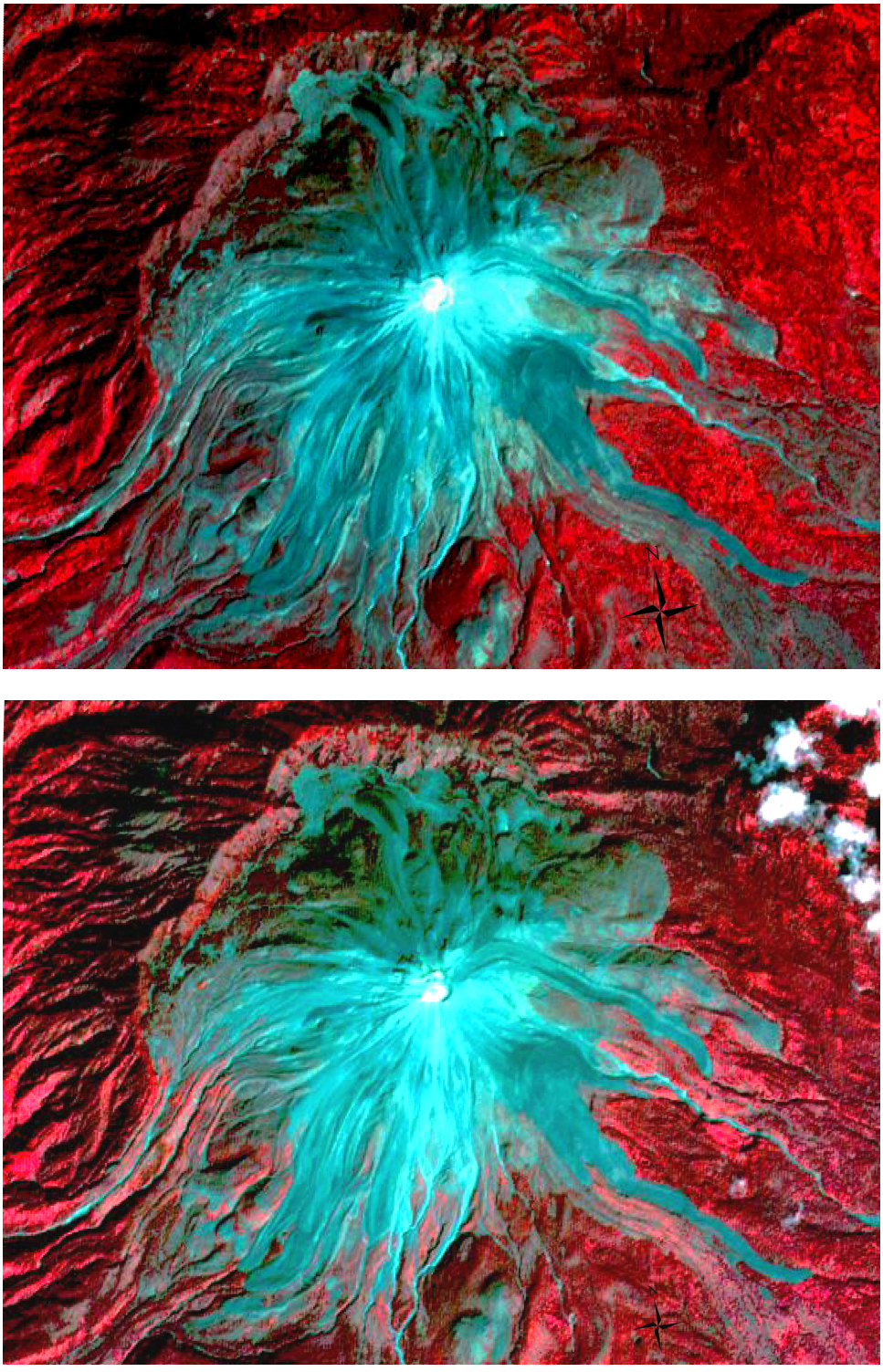

Figure 18: ASTER VNIR images: March 9, 2009 (top), November 14, 2009 (bottom).

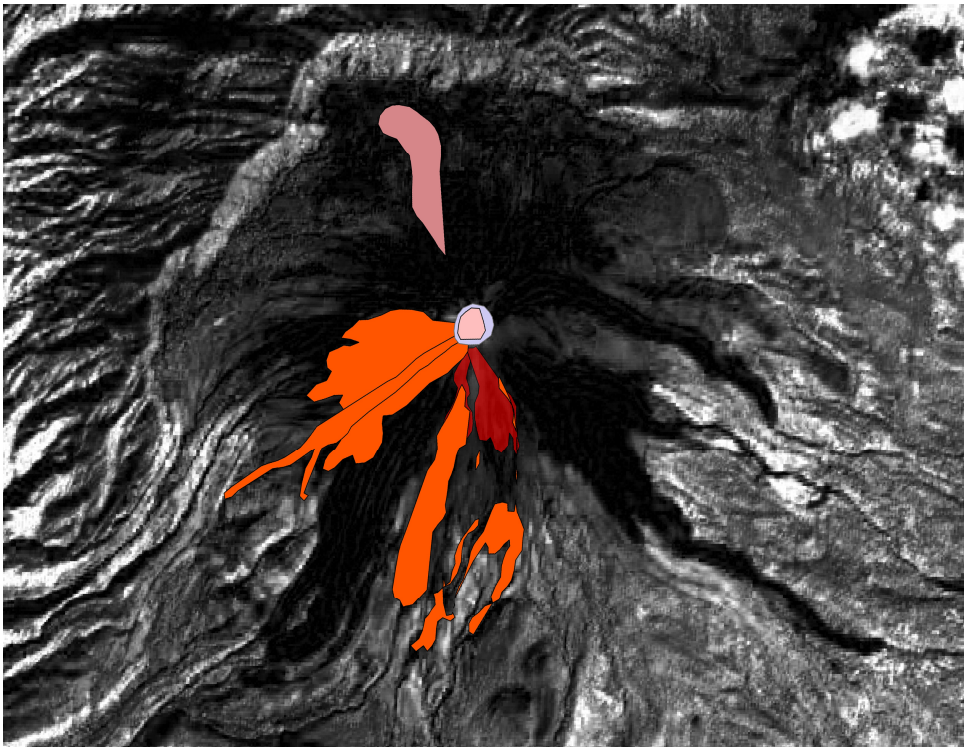

Figure 19: Map of changes that occurred between the previous pair of images (Figure 18). The lava dome measured 231 m in March 9, 2009 and in November 14, 2009 the dome measured 244 m and is outlined in pink. The crater is outlined in purple; the 2004 flow is outlined in pink. Subsequent flows are outlined in orange

Table 2: Summary of Volcán de Colima's activity. Date of ASTER scene showing Volcán de Colima along with whether there was lava dome detected and the diameter of the dome. "Y" indicates yes, and "N" indicates no in reference to whether a dome could be observed.

Date of ASTER Scene	Lava Dome Detected?	Diameter
March 19, 2003	Y	108 m
May 6, 2003	Y	275 m
October 29, 2003	Y	311 m
March 8, 2005	Y	122 m
April 9, 2005	Y	128 m
November 3, 2005	N	–
January 6, 2006	N	–
February 7, 2006	Y	100 m
March 11, 2006	N	–
April 12, 2006	Y	78 m
November 26, 2006	N	–
January 9, 2007	N	–
February 26, 2007	Y	75 m
March 30, 2007	Y	95 m
April 15, 2007	Y	120 m
December 11, 2007	Y	142 m
March 16, 2008	Y	210 m
April 1, 2008	Y	197 m
May 3, 2008	Y	178 m
December 13, 2008	Y	228 m
March 9, 2009	Y	231 m
November 14, 2009	Y	244 m

DISCUSSION

Lava Dome and Crater Vesicularity

As previously stated, vesicularity can be used to infer pre-eruptive conditions and is affected by the volatile content, emplacement time, and internal structure of a flow. It should be noted that the vesicularity interpretation could be attributed to any small-scale roughness elements, as pointed out by Byrnes et al. (2004). However, in the context of this study, it is likely that the vast majority of small-scale roughness elements are vesicles, given the composition of the dome.

During a constructive phase, magma that is low in volatiles rises and forms a new dome. The low abundance of volatiles leads to a decrease in vesicularity (Figure 4). Specifically, decreases in the maximum calculated vesicularity are evident in the March 19, 2003, March 8, 2005, February 7, 2006, and April 12, 2006 data. Based on the given data, all four dates occur during a period where the dome was in a constructive stage. The possible exception is March 8, 2005. It has been indicated that in the months leading up to the large explosive event in June 2005, the dome filled the crater (Varley et al., 2009). According to measurements taken for this study, the dome during that time measured close to 122 meters in diameter, whereas the crater measured ~285 m.

Despite the apparent discrepancy in dome size, the ASTER data clearly demonstrates that there was a decrease in vesicularity at the time of an already formed dome. A possibility for decreased vesicularity during the presence of a dome may be due to minor explosive events. These explosions produce ash that can fill in vesicles, leading to a decrease in vesicularity exposed at the surface. Additionally, very fine particles, such as ash, tend to produce fairly flat spectra, which would then be interpreted (based on the methodology) as being low vesicularity. It appears that when there is a decrease in volatiles, thus a decrease in vesicularity, the lava dome is undergoing a constructive phase.

Once a dome has formed, there is an increase in pressure due to the decompression of the magma, resulting in small Vulcanian or Peléan explosions that destroy the dome (N. Varley, personal communication, 2010). These Vulcanian or Peléan explosions signal the end of each short-term phase within longer-term eruptive cycles. Based on the ASTER data, vesicularity is low during constructive phases and then vesicularity increases during destructive phases. This increase could be attributed to removal of ash cover, such as exposing the vesicular dome interior due to rock fall events. This is evident during the activity of 2005 and more recently the activity in 2008 (see Figure 6).

Lava Dome and Crater Temperature

When examining changes in surface temperature of the volcanic dome and inside the crater, it is important to note that each ASTER data value represents a pixel-integrated temperature. However, each pixel does not fall exactly in the area of interest. For

instance, when measuring the crater, it is possible to have some of the pixel area include the sides of the volcano. Similarly for the dome, some of the area located in the pixel may be an area of the crater, not just the dome. For this study, the maximum temperature was of most interest.

Examining changes in dome temperature, it appears that temperatures are at a maximum before an eruptive event, which may relate to incandescent material being extruded at the edge of the dome. This can be seen during April 9, 2005, April 12, 2006, and March 30, 2007 (Figure 7). Based on this study, and information provided by the GVP archived reports, all three of these dates are during a time when dome diameter was at a maximum before an eruption (seen in April 9, 2005) or during a period of resurgence (seen in April 2006 and March 2007). It has been hypothesized that temperatures on the dome are possibly being controlled by cooled material accumulating on the top of the dome as it grows (Varley et al., 2009). This suggests that as new material is extruded onto the dome (i.e., exogenous growth), the surface temperature will show an increase and then once this material is cooled and a crust is formed, the dome surface temperature decreases, as further growth is predominantly endogenous. Immediately after the lava dome is removed by an explosive event, a decrease in temperature is observed. Once activity resumes, the crater shows an increase in temperature, as seen in November 2005. Another explanation of the observed increase in temperature is that it is due to increased heat flow coming out of the vent, as molten material is moving up to the surface prior to the eruption. This would allow for an increase in temperature to be detected without the visible presence of incandescent material. The fluctuating temperature is indicative of the flux in volcanic activity through time.

Morphological Changes

The changing shape of the volcanic crater and dome provide additional clues as to how strong an eruption may have been. Crater edges undergo subtle changes due to explosive events, effusion of lava, and slope failure of crater walls. Changes in the morphology can be attributed to explosive events, seen from March 19, 2003 to May 6, 2003 as well as April 2005 to November 2005. Explosive eruptions between these dates enlarged the crater's diameter. Morphological changes on the dome can be due to explosive events, gravitational collapse, and factors effecting the endogenous and exogenous growth of the dome, such as vertical growth building the dome upwards instead of through cracks on the side of the dome, which would build it out more horizontally. Factors affecting the morphological changes on the flanks of the volcano are much more related to external processes. Many of the changes that occur on the flanks of Volcán de Colima are due to pyroclastic material or emplaced lava flows and lahars. The morphological changes that were determined all appear to correlate with an eruption or emission of lava or pyroclastic material during that time. It is apparent that the lava dome and crater change shape over time and are dependent on the volcanic activity.

Two major limitations that were encountered during this study were the limited published ground-based data and the fact that ASTER is a targeted instrument. Additional ground-based data would have been extremely useful in order to have accurate observations on a more frequent basis rather than observations made only when an ash or steam plume was observed. Having ground-based data to compliment satellite data is extremely important and helpful, as was shown by the utility of the Smithsonian GVP reports. ASTER is a very useful instrument, however because ASTER is a targeted instrument, only limited

data is acquired for a given target. Typically, ASTER data is acquired for volcanic targets in response to other observations, but regular acquisition of ASTER data would benefit monitoring efforts.

CONCLUSIONS

Satellite data provides a synoptic view allowing for observation of new activity to be observed earlier than ground-based data may allow, as shown in this study. The use of satellite remote sensing allows for data, such as small-scale roughness, surface temperature, and visible observations to be readily available in order to gain further understanding of a volcano's behavior. In the case of the Volcán de Colima, satellite remote sensing provides insight to the constructive and destructive phases of the lava dome. Using ASTER data, the growth and destruction of the lava dome was clearly visible during times when traditional ground-based data did not detect a growing lava dome. The observation of a new lava dome in 2006 was detected in multiple ASTER scenes in the course of this study, whereas the first previous documentation of this lava dome was not reported until early 2007.

This study demonstrates the utility of using satellite-based remote sensing on active volcanoes apart from the capacity of ground-based data collected. By examining ASTER data, early detection of a new lava dome can be determined as well as vesicularity and temperature changes associated with the lava dome that may precede significant eruptions. This could lead to better understanding of when constructive and destructive

phases start and finish. The current activity at Volcán de Colima shows a large dome with explosive eruptions occurring daily. Based on this research, one could conclude that Volcán de Colima is currently in a destructive cycle (as of December 2010), which will eventually end in the destruction of the dome, whether it is a large explosive eruption or effusive event. By looking at the past activity and available supplementary ground-based data, satellite remote sensing can provide increased monitoring measures worldwide.

REFERENCES

Abrams, M., Glaze, L., and Sheridan, M., 1991. Monitoring colima volcano, Mexico, using Satellite data. Bulletin of Volcanology. 53, 571-574.

Byrnes, J.M., Ramsey, M.S., and Crown, D.A., 2004. Surface unit characterization of the Mauna Ulu flow field, Kilauea Volcano, Hawai'i, using integrated field and remote sensing analyses. Journal of Volcanology and Geothermal Research. 135, doi:10.1016/j.jvolgeores.2003.12.016, 169-193.

Cruz-Reyna, S.D.L., 1993. Random patterns of occurrence of explosive eruptions at Colima Volcano, Mexico. Journal of Volcanology and Geothermal Research. 55, 51-68.

Francis, P., and Rothery, D., 2000. Remote sensing of active volcanoes. Annual Review of Earth and Planetary Sciences. 28, 81-106.

Garduno V.H., and Tibaldi A., 1991. Kinematic evolution of the continental active triple junction of the western TMVB. C.R. Academy of Science, Paris, 312, 135-142

Gonzalez, M.B., Ramirez, J.J., and Navarro, C., 2002. Summary of the historical eruptive activity of Volcán De Colima, Mexico 1519-2000. Journal of Volcanology and Geothermal Research. 117 (1-2): 21-46.

Guzman, E.J., and de Cserna, Z., 1963. Tectonic history of Mexico: Backbones of the Americas. American Association of Petroleum Geologists, Memoir 2: 113-130.

Luhr, J.F., and Carmichael, I.S.E., 1980. The Colima Volcano Complex, Mexico. Contributions to Mineralogy and Petrology. 71: 343-372.

Luhr, J.F., Nelson, S.A., Allan, J.F., and Carmichael, I.S.E., 1985. Active rifting in southwestern Mexico: Manifestation of an incipient eastward spreading-ridge jump. Geology 13(1): 54-57.

Macias, J.L., 2007. Geology and eruptive history of some active volcanoes of Mexico. Geology of Mexico : Celebrating the centenary of the geological society of Mexico. A.N.-S. Susana A., Alaniz - Alvarez. Boulder, Geological Society of America. 422.

Oppenheimer, C.M.M., and Rothery, D.A., 1991. Infrared monitoring of volcanoes by satellite. Journal of the Geological Society. 148(3): 563 - 569.

Pieri, D., and Abrams, M., 2004. ASTER watches the world's volcanoes: A new paradigm for volcanological observations from orbit. Journal of Volcanology and Geothermal Research 135(1-2): 13-28.

Ramsey, M., andDehn, J., 2004. Spaceborne observations of the 2000 Bezymianny, Kamchatka eruption: The integration of high-resoultion ASTER data into near real-time monitoring using AVHRR. Journal of Volcanology and Geothermal Research. 135: 127-146.

Ramsey, M.S., and Fink, J.H., 1999. Estimating silic lava vesicularity with thermal remote sensing: A new technique for mapping and monitoring. Bulletin of Volcanology. 61: 32-39.

Robin, C., Philippe, M., Camus, G., Cantagrel, J.-M., Gourgaud, A., and Vincent, P.M., 1987. Eruptive history of the Colima Volcanic Complex (Mexico). Journal of Volcanology and Geothermal Research. 31: 99-113.

Robin, C., Camus, G., and Gourgaud A., 1991. Eruptive and magmatic cycles at Fuego de Colima Volcano (Mexico). Journal of Volcanology and Geothermal Research. 45: 209-225.

Varley, N.R., Arambula, R., Lavallée, Y., Bernstein, M., Ryan, A.G., and Maskell, A., 2009. Magma ascent and lava dome evolution at Volcán de Colima, Mexico. American Geophysical Union, Fall Meeting, (Abstract #V12A-05).

Venzke, E., Wunderman, R.W., McClelland, L., Simkin, T., Luhr, J.F., Siebert L., Mayberry G., and Sennert, S. (eds.), 2010. Global Volcanism, 1968 to the Present. Smithsonian Institution, Global Volcanism Program Digital Information Series, GVP-4 (http://www.volcano.si.edu/reports/).

Walker, G.P.L. 1973. Explosive volcanic eruptions – a new classification scheme. International Journal of Earth Sciences. 62: 431-446.

Welch, R., Jordan, T., Lang, H., and Murakami, H., 1998. ASTER as a source for topographic data in the late 1990's. IEEE Transactions on Geosciences and Remote Sensing. 36(4).

Yamaguchi, Y., Kahle, A. B., Tsu, H., Kawakami, T., and Pniel, M., 1998. Overview of Advanced Spaceborne Thermal Emission and Reflection Radiometer. IEEE Transactions on Geosciences and Remote Sensing. 36(4): 1062-1071.

APPENDICES

Appendix I

The following ASTER VNIR images (Figures A1-A4) show data for additional dates. These data supplement the volcanic history illustrated in Figures 8-19.

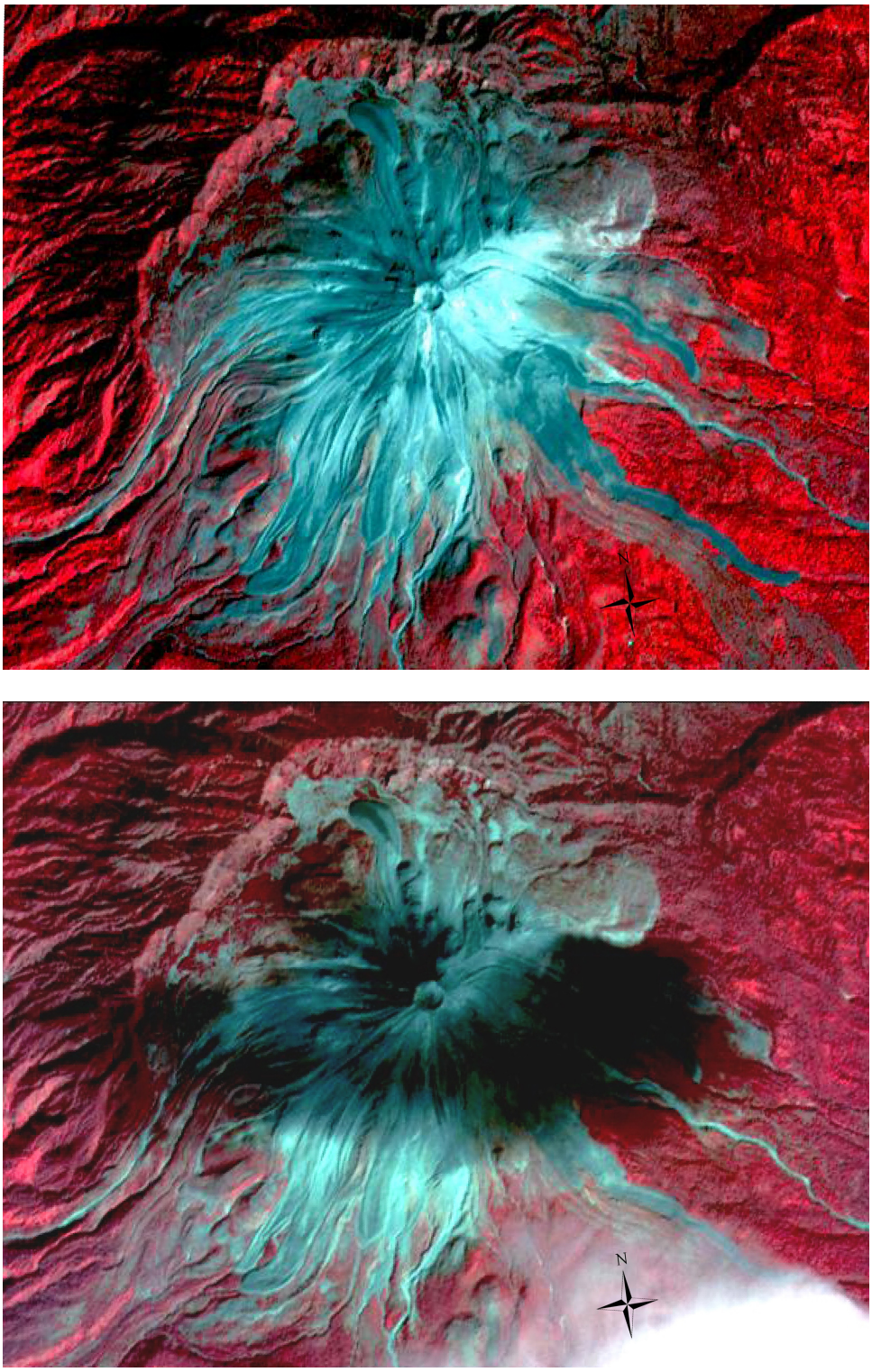

Figure A1. ASTER VNIR images: April 19, 2005 (top), November 3, 2005 (bottom).

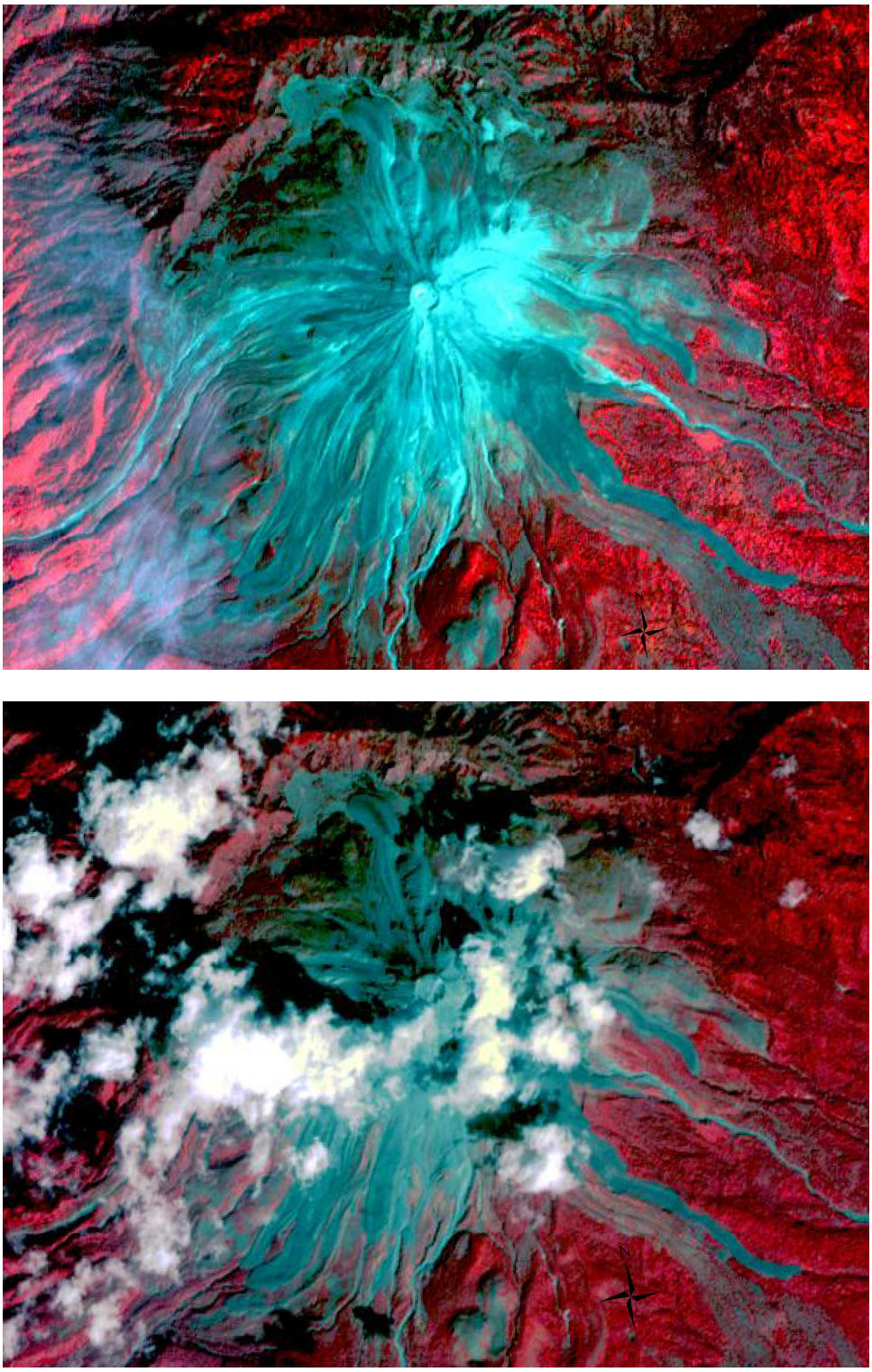

Figure A2. ASTER VNIR images: January 9, 2007 (top), April 15, 2007 (bottom).

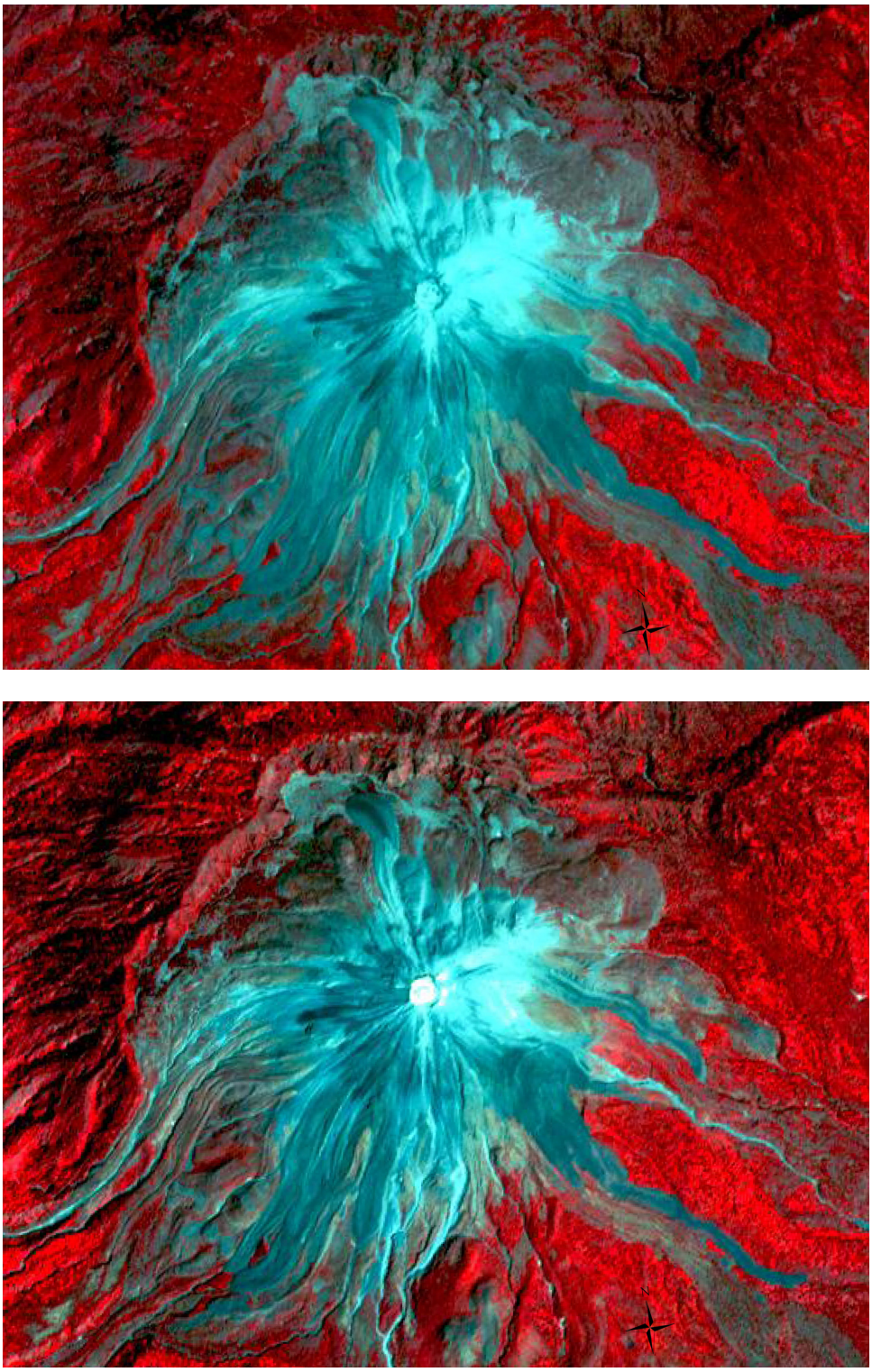

Figure A3. ASTER VNIR images: February 26, 2007 (top), March 16, 2008 (bottom).

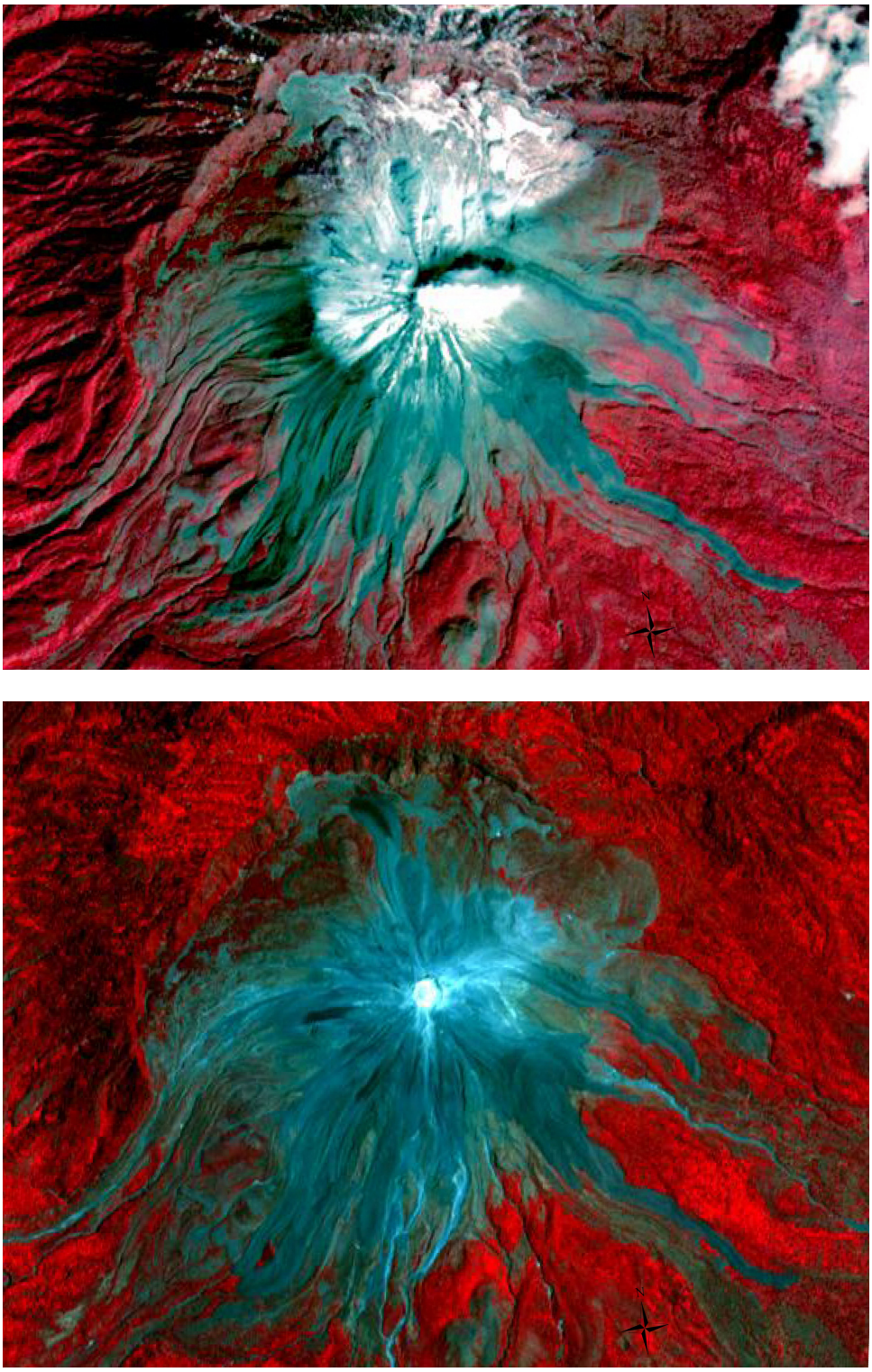

Figure A4. ASTER VNIR images: April 1, 2008 (top), May 3, 2008 (bottom).

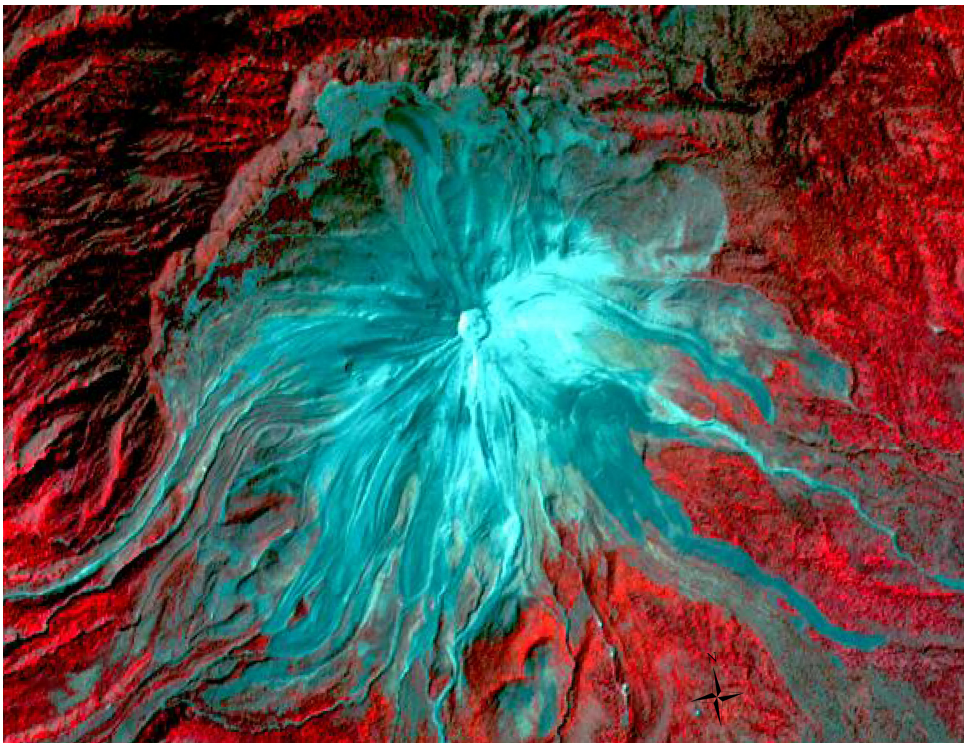

Figure A5. ASTER VNIR image: December 13, 2008.

VITA

Maggie Lin Silvertooth

Candidate for the Degree of

Master of Science

Thesis: MONITORING ACTIVE VOLCANISM USING ASTER SATELLITE REMOTE SENSING: VOLCÁN DE COLIMA, COLIMA, MEXICO

Major Field: Geology

Biographical:

Education:

Completed the requirements for the Master of Science in Geology at Oklahoma State University, Stillwater, Oklahoma in December 2010.

Completed the requirements for the Bachelor of Science Geology at Oklahoma State University, Stillwater, Oklahoma in June 2008

Experience:

Presented at Geological Society of America Annual Meeting, Denver, Colorado: October 2009
Presented at International Association of Volcanology and Chemistry of the Earth's Interior: Colima, Mexico: February 2009

Professional Memberships:

American Association of Petroleum Geologists – Student Member
Association of Women in Geosciences – President
Geology Graduate Student and Professionals Association – Vice President
Oklahoma State Geological Society – Student Member

Name: Maggie Lin Silvertooth Date of Degree: December, 2010

Institution: Oklahoma State University Location: Stillwater, Oklahoma

Title of Study: MONITORING ACTIVE VOLCANISM USING ASTER SATELLITE REMOTE SENSING: VOLCÁN DE COLIMA, COLIMA, MEXICO

Pages in Study: 46 Candidate for the Degree of Master of Science
Major Field: Geology

Scope and Method of Study: ASTER satellite data was collected and analyzed in order to quantify changes in temperature, vesicularity, and morphology of the dome and crater that support evidence of constructive and destructive phases of lava dome growth and destruction cycles. These cycles are characterized by sporadic growth of a lava dome that is subsequently destroyed by a Vulcanian or Pelean style eruption. Activity reports were compared with ASTER images and new deposits were mapped along the flanks of the volcano. There is no way to distinguish between pyroclastic material, rockfall deposits, lahar deposits or lava flows therefore all new flows were mapped.

Findings and Conclusions: During a constructive phase, magma that is low in volatiles rises and forms a new dome. The low amount of volatiles leads to a decrease in vesicularity. Therefore during a destructive phase vesicularity is increased. Examining changes in temperature on the dome, it appears that temperatures are at a maximum before an eruptive event, such as incandescent material being extruded at the edge of the dome. Immediately after the lava dome is removed by an explosive event, a decrease in temperature is observed. Once activity resumes, increase in temperature is seen. Morphological changes on the dome can be due to explosive events, gravitational collapse, and factors affecting the endogenous and exogenous growth of the dome. Satellite data provides a synoptic view allowing for observation of new activity to be observed earlier than ground based data may allow. In the case of the Volcán de Colima, satellite remote sensing provided insight to the constructive and destructive phases of the lava dome and current activity.

Name: Maggie Lin Silvertooth Date of Degree: December, 2010
Institution: Oklahoma State University Location: Stillwater, Oklahoma

ADVISER'S APPROVAL: Dr. Jeffrey M. Byrnes